Potential use of matakaolin as a partial replacement of preformulated lime binder to improve durability of hemp concrete under cyclic wetting/ drying aging

Redouane Zerrouki, Amar Benazzouk, Matthieu Courty, Haikel Ben Hamed

Version of Record: https://www.sciencedirect.com/science/article/pii/S0950061822010662
Manuscript_b80837f78b902fc54b27dfaf1a3996e2

Potential use of matakaolin as a partial replacement of preformulated lime binder to improve durability of hemp concrete under cyclic wetting/drying aging

R. Zerrouki [a,*], A. Benazzouk [a], M. Courty [b], H. Ben Hamed [a]

[a] Laboratoire des Technologies Innovantes (UR/UPJV 3899), Université de Picardie Jules Verne / Avenue des Facultés-Le Bailly – 80025 Amiens Cedex 01, France

[b] Laboratoire de Réactivité et Chimie des Solides UMR CNRS 7314, Université de Picardie Jules Verne/ 33, Rue Saint Leu 80039 Amiens

* Corresponding author

E-mail address: redouane.zerrouki@etud.u-picardie.fr (R. Zerrouki)

Abstract

This study reports the experimental investigation of a commercial formulated lime binder (Tadical PF70) modification effect on the durability of hemp concrete specimens when subjected to continuous wetting and drying cycles. The influence of partial replacement of Tradical PF70 binder by metakaolin has been studied by testing the physico-mechanical properties of samples including mass loss, porosity, compressive and flexural strengths, and corresponding toughness for aging conditions of 15, 25, and 50 wetting/drying cycles. Considered as a critical factor which contributes to the specimen deterioration, a separate investigation of the degradation rate of the embedded hemp particles in specimens at aging cycle intervals has been also performed. The results have shown that the pozzolanic reaction of amorphous silica contained in metakaolin with dissolved calcium hydroxide appears to significantly minimise the degradation of hemp concrete. The corresponding reaction consumes calcium hydroxide to produce hydrated calcium silicates and in turn will lead to the lowest alkalinity of pore solution which is considered as the main responsible for hydrolysis of hemp particles. The examination of the relationship between embedded hemp particle deterioration degree and the loss of mechanical properties of hemp concrete has shown that the use of metakaolin is an effective means to improve durability of specimens mainly through the restraint of hemp particle degradation.

Keywords: Hemp concrete, Metakaolin, Durability properties, Wetting/Drying cycles, Degradation mechanisms, Mineralisation of embedded hemp, Micro-analyses.

1 Introduction

The promotion of vegetable materials in the construction field and the problems related to the environmental issues have motivated extensive research works on eco-friendly materials. In this respect, the reduction of energy consumption and the use of vegetable raw materials as mineral aggregates replacement are the most important elements [1]. To meet this challenge, the construction industry must convert its construction practices to provide innovative materials that meet the new requirements of users in terms of environmental concerns and comfort. Given their environmental friendliness and availability, particular interest has been addressed to the use of aggregates and/or fibers derived from vegetable sources in composite materials including flax, hemp, rapeseed, coir, jute, bamboo, pineapple leaf, date palm, kenaf, alfa to give rise to several applications [2-6]. The results highlighted the benefits of the characteristics of bio-composite specimens such as interesting physico-mechanical properties, reduction in the thermo-acoustic transfer, and low density. The use of these materials is interesting as they exhibit a set of important advantages such as their wide availability at relatively low cost, bio-renewability, ability to be recycled, biodegradability, non-hazardous nature, low carbon footprint.

According to the literature, extensive studies have focused on the concrete-based hemp particles as nonstructural construction materials. This innovative bio-based material in which hemp shives are mixed with a binder (mainly lime) and in rare cases additional compounds, is very widespread in France and has a regulatory framework for its use in the construction sector [7, 8]. Several studies conducted on the physico-mechanical properties of hemp concrete also called "hempcrete" have shown that the material exhibit a compressive strength ranged from 0.2 to 0.8 MPa mainly depending on the density and binder type [9, 10]. To increase the mechanical performances, other studies have been focused on the effect of the binder type, hemp particle size, and particles-matrix interfacial bond [11, 12]. Results have shown that the addition of pozzolanic material and other compounds to binder allows increasing the compressive strength of hemp concrete at an early age, where the pozzolanic products promote a high adherence of particles to the matrix. The optimisation of the mechanical properties of concrete via the orientation of hemp shives and the compaction method can also affect the thermal performances, while the specimen exhibited a dry thermal conductivity varied from 0.062 to 0.125 W/mK, depending on its density [13-15]. Another study focused on hemp concrete based silica sol binder has shown that the specimen achieved a thermal conductivity of 0.053 W/mK, without compromising its mechanical strengths compared to low and medium density hemp concretes [16]. In addition, the hemp concrete offers a healthy and high quality living environment, evidenced by the vegetable material capability to regulate indoor humidity of buildings by absorbing and/or releasing water [17-19]. However, the dynamic hygric behaviour of hempcrete contributes to a significant level of moisture buffering that avoids excessive energy loss due to ventilation [20].

In the same way, composites-based other bio-aggregates such as straw bales and rapeseed straw, corn stalk, jute straw, Diss, and rice husks mixed with different binder types have been found to be energy efficient materials thus providing lightweight concrete with high insulation performances [21-24].

Despite the mentioned beneficial properties of construction materials based vegetable particles, their use in hydraulic binder is limited by their low durability in alkaline environment. When exposed to the alkaline pore solution, the properties of vegetable particles can deteriorate causing their embrittlement. This results in a notable decrease in their pull-out resistance in the binder matrix, thereby compromising the durability of concrete sample. In addition, the hydrophilic nature and the high water absorption of vegetable particles are other disadvantages that affect the mechanical and thermal performances of specimens. The degradation problem related to the vegetable particle embrittlement results from a combination of alkali-attack and mineralisation effects due to the migration of hydration products to lumen [25, 26]. The degradation mechanism has been identified according to three sequences of damage: (i) appearance of the void space at interfacial zone between vegetable particles and binder matrix resulting from their alternative swelling and shrinking under cyclic wetting and drying effect; (ii) migration of dissolved hydrate components in water through the interfacial zone, while the vegetable particles absorb the dissolved components; (iii) after water evaporation at drying phase of cycle, free Ca^{2+} ions precipitate on the surface and then infiltrate the cell walls and lumen cavity of vegetable particles, thus causing their mineralisation [27]. The other main factor affecting the durability of embedded vegetable materials is related to the higher alkalinity of pore solution in hydraulic binder media (pH> 13), caused mainly by the presence of OH^- in the interstitial water. The alkaline pore water dissolves the lignin, hemicellulose, and cellulose constituents thus inducing the degradation of particles [28].

To restrain the degradation of vegetable particles in alkaline medium, several approaches have been studied and reported in the literature. The selected two methods include: (i) Modification of hydration products in the matrix by using supplementary binder in order to reduce and/or remove the alkaline compounds [29, 30]. However, two basic treatments leading to consume calcium hydroxide in the matrix can be used: adding pozzolanic compounds will promote the transformation of calcium hydroxide into C-S-H crystals thus reducing the alkalinity of binder matrix; accelerated carbonation allows calcium hydroxide to react with carbon dioxide (CO_2) thus resulting in $CaCO_3$ hydrates formation, which contributes to increase the mechanical strengths of the specimen. (ii) Physical and/or mineralogical modification of the vegetable materials with the aim of improving the particle–matrix interfacial bond, though the physical and/or chemical pretreatment which also serves as a protective barrier.

Several studies have shown the direct effect of calcium hydroxide on vegetable fiber degradation, inducing the loss of durability of reinforced cement-based composites [31-34]. The effect of alkaline attack on the durability of sisal and coconut fibers has been evidenced by their immersion in a highly alkaline media of calcium hydroxide [26]. The results have shown that after 300 days of immersion, the fibers lost in their flexibility due to the crystallisation of lime in the lumen and cell walls of the fibers. The results also show that the degradation of fibers is less extent when immersed in sodium hydroxide solution, due to its low alkalinity degree. To restrain the alkaline media attacks of cement composite based on vegetable fibers, Toledo-Filho et *al*. [35] studied the effect of partial replacement of cement Portland by silica fume and blast-furnace slag. The results have shown that the silica fume is more effective in slowing the strength loss of the cement composites due to its high chemical reactivity, compared to the blast-furnace slag materials. To enhance the durability of composite-based softwood kraft pulp fiber when subjected to wet/dry cycles, a variety of supplementary cementitious materials such as silica fume, blast furnace slag, fly ash, and blends of raw and calcined diatomaceous earth have been used [36, 37]. The results highlighted the effectiveness of different supplementary materials to prevent the composite degradation at different level extents. In the same way, similar study has shown that the use of calcined crushed clay brick as a partial replacement of cement in concrete produced a binder completely free in calcium hydroxide due to the pozzolanic reaction [38]. As reported in the literature, other procedures may be effective in enhancing the durability of vegetable materials, like silane coating, hornification, autoclave, thermal treatment, sodium silicate and silicate potassium treatments [39-41]. The effect of some treatments (beating, bleaching, initial drying process) of softwood kraft pulp fibers on composite degradation has been analysed by several authors [42]. The results highlighted the beneficial effect of thermo-mechanical treatment on minimising composite degradation, evidenced by more slowly decrease in mechanical strengths.

This paper deals with the investigation of hemp concrete durability when subjected to wetting and drying cycles. In contrast to previous works reported in the literature, which generally evaluate the degradation of vegetable concrete by testing the loss of their mechanical properties, only a few works addressed the separate deterioration of embedded vegetable materials in specimens. In this study, the effect of partial replacement of commercial pre-formulated lime binder (Tadical PF70) by metakaolin on the durability of hemp concrete subjected to continuous wetting and drying cycles has been studied. The degradation level has been assessed by examining the variation of physico-mechanical properties, including mass loss, porosity, compressive and flexural strengths, and corresponding toughness for aging conditions of 15, 25, and 50 wetting/drying cycles, compared to the reference specimens without aging cycles, tested at 28 days. Considered as one of the main

factors leading to the specimen deterioration, a separate approach has been used to evaluate the degradation mechanism of embedded hemp particle by analysing its composition change, surface morphology and microstructure modifications, and crystalline properties variation along wetting and drying cycle intervals. This work also allows the description of the metakaolin addition effect on the degradation resistance of embedded hemp particles under a combination effect of alkali-attack and mineralisation mechanisms.

2 Materials and methods

2.1 Materials

2.1.1 Preformulated lime binder (Tadical PF70)

The binder used in this study is a commercial product widely used in the production of hemp concrete, called "Tradical PF70". It consists of 75% air lime, 10% hydraulic lime, and 15% of pozzolan mixture, produced by "Lhoist" industry in the Northern region of France [43]. The advantage of this material is related to the hydrophobic nature of air lime which acts as a protective barrier for included vegetable particles, against physical and chemical degradations when specimens exposed to hygroscopic environment. The used binder exhibits 720 ± 20 kg/m^3 in bulk density, as measured by filling container of 1 liter in volume and weighing.

2.1.2. Metakaolin/ARGICAL-M 1000

The metakaolin used in this study, as additive to Tradical PF70 binder, was supplied by Imerys Refractory Minerals Industry [44]. It consists of an artificial pozzolan obtained by calcining and micronising kaolinite clay from the region of Charentes Basin in France. Called "ARGICAL-M 1000" and has a chemical formula of $Al_2O_3.2SiO_2$, it is an amorphous non-crystallised material with a maximum particle size of 0.063 mm. This material exhibits a high potential for use as additive in binder considering its high pozzolanic reactivity. The metakaolin chemical composition and physical properties are reported in Table 1.

Table 1

Chemical composition and physical properties of metakaolin pozzolan [44]

Chemical composition/Physical properties	**Value**
SiO_2	59.00 %
Al_2O_3	36.30 %
Fe_2O_3	1.40 %
CaO	0.10 %
MgO_3	0.10 %
Pozzolanic Activity index (28 days)	1.03
Specific area (BET)	20 m^2/g

Bulk density	400 kg/m^3
Specific gravity	2400 kg/m^3

2.1.3. Hemp particles

The hemp shivs are ligneous particles extracted from the core of hemp stems (cannabis sativa). The used particles are by-products derived from defibration process of textile industry and supplied by "La Chanvrière De L'aube", which is located in the central region of France. The shape of hemp shivs is shown in Fig. 1a. As shown in Fig. 1b, the ellipse shape of hemp particles (flat and elongated form), leads to high difficulty to characterise their size distribution using the mechanical sieving. Therefore, it is necessary to consider other methods like image analysis using dedicated software which gives the middle width and length measurements by assimilating particle to an ellipse. The image analysis method has been already used to characterise the internal structure of materials [10]. In this study, the equivalent size is defined as the ratio between the width and the length of hemp particle which has been measured using "Image J" software [45]. A 10 g sample of hemp shivs was prepared and two-dimensional VD imaging is conducted by taking physical sections of the material and imaging the exposed face using a digital camera. To identify the shivs within the images, a threshold filter has been used to segregate the smoothed image, thus producing a binary picture which serves to measure the width and the length for hemp particles. The equivalent size distribution of hemp particles is shown in Fig. 1c.

As shown in Fig. 2, the SEM micrographs of the cross-section show a porous and complex structural morphology with size ranged from 10 to 50 µm of the cells. It can also be observed that the pores are organized in capillary form, thus making the reinforcement specimen highly performed as regards thermal insulation. However, the rough surface of hemp particle will result in a high bond between particles and binder matrix.

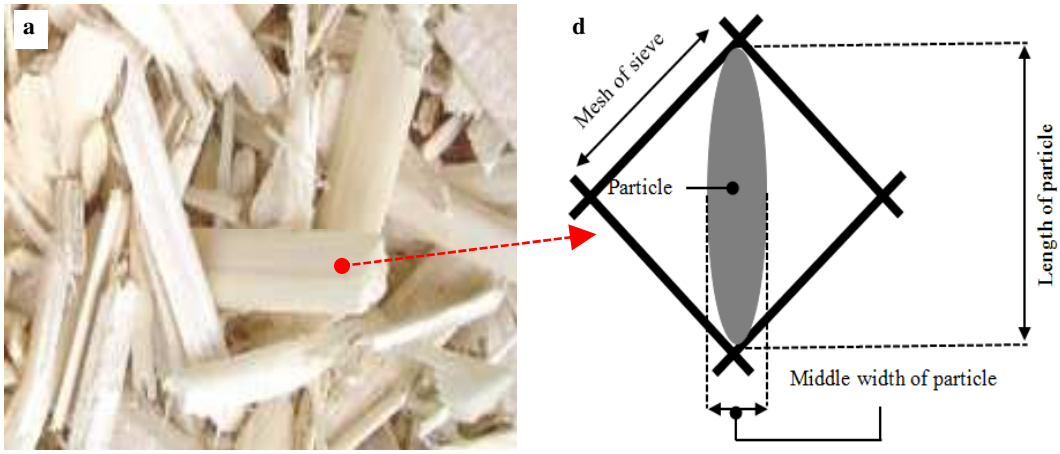

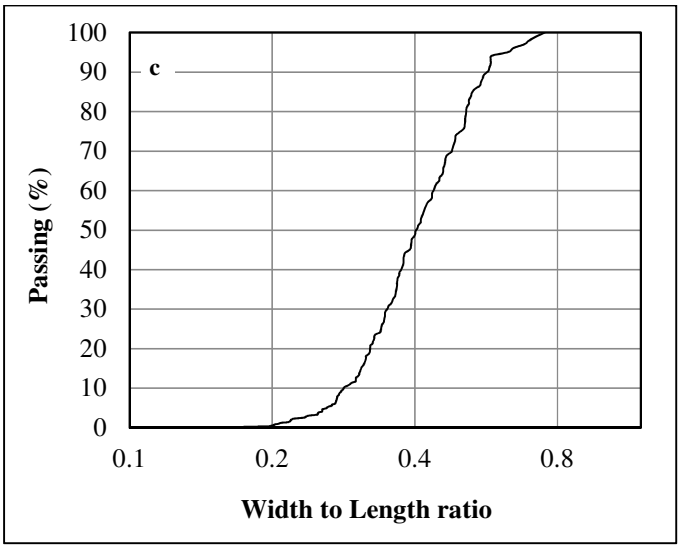

Fig. 1. (a): Hemp shivs aspect, (b): Ellipsoid form of hemp particles, (c): Equivalent size distribution of hemp

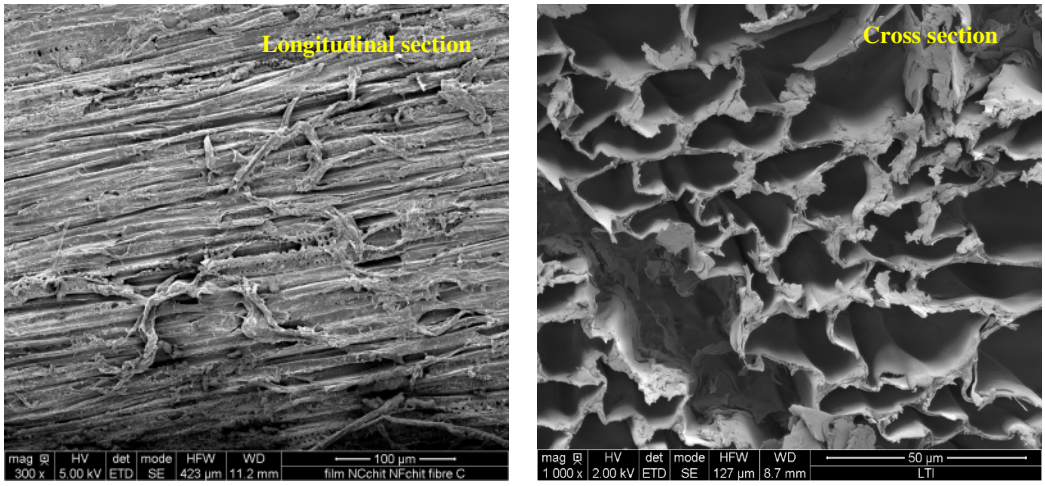

Fig. 2. SEM observations of longitudinal and cross section morphology of hemp particle

Different test measurements were performed to characterise the properties of hemp particles, including bulk and absolute densities, porosity, and water absorption.

- The bulk density ρ_{bulk} *(in kg/m^3)* of particle has been determined after drying in an oven at 70 °C. The measurement involves filling container of 1 liter in volume, and levelled on the top surface before weighing. The average result of three measurements was obtained from the ratio of mass particles to the volume of the container.
- The absolute density ρ_{abs} *(kg/m^3)* measurement has been carried out according to the protocol described in several research works [46]. The hemp particles were milled in powder form and dipped in cyclohexane, while the mix was degasified in order to evacuate air contained in the porous structure of particles. After reaching a constant volume of cyclohexane in the pycnometer, the absolute density was determined using Eq. 1.

$$\rho_{abs} = \frac{M_D}{M_{D+C} - (M_C/\rho_C)} \quad (1)$$

Where: ρ_c (kg/m^3) is the density of cyclohexane, M_D, M_{D+C} and M_C (g) are the masses of hemp, pycnometer (cyclohexane + saturated hemp), and cyclohexane, respectively.

- The total porosity ϕ_D(%) of hemp was determined as regards their absolute and bulk densities defined below, by using Eq. 2.

$$\phi_D = \left(1 - \frac{\rho_{bulk}}{\rho_{abs}}\right).100 \quad (2)$$

- The water absorption capacity was evaluated by drying the particles in a dry oven at 70 °C, before their immersion in tap water. After reaching a constant mass, the water absorption was determined considering the dry and total saturated masses of hemp particles.

The properties of flax particles are summarised in Table 2, where the reported values are the average test results of three replications. These results are similar to that obtained by Rahim et *al.* [47] using the same supplied particles.

Table 2

Hemp particle properties

Bulk density (kg/m^3)	**Absolute density (kg/m^3)**	**Porosity (%)**	**Water absorption (%)**
105 ±20	1256 ±150	91 ±5	337 ±25

2.1.4. Specimen production

The hemp concrete specimens were produced by initially mixing binder and water in a planetary mixer. The hemp particles were then uniformly dispersed with slow increase throughout the mix to overcome the balling effect. Two groups of specimens were made with the same mixture proportions of 1:2:1 by volume of binder, hemp particles, and water, respectively, according to the "Professionals Rules of Hempcrete Work Execution" recommendations [48]. For the experiments, two different binder compositions were selected to compare the response of the specimens under laboratory tests. The first group of specimens (HCS samples) was elaborated with a commercial preformulated lime-based binder, while for the second group, 20% volume of Tradical PF70 was replaced by metakaolin (HCMS samples). All specimens were made of a mixture with hemp to binder (with and without metakaolin) volume ratio of 1:2 in order to achieve a density ranged from 580 to 650 kg/m^3.

After mixing, the fresh specimen was filled in two layers into cylindrical (110 × 220 mm) and prismatic (70 × 70 × 280 mm) steel molds and then immediately compacted using a static compaction process, performed

by a hydraulic press (Fig. 3a). In order to prevent the stress relaxation, all composition mixes were kept under compaction load for 30 h, with a maximum stress of approximately 0.25 MPa. The corresponding diagrams of applied stress vs. time curve for specimens are shown in Fig. 3b. After 24 h, all samples were demolded and moist-cured under a temperature of 20 ± 2 °C and 98% relative humidity conditions, for 28 days before testing. For each group, three identical specimens were produced and tested. The 28-days dry density of produced specimens are 530 kg/m^3 and 520 kg/m^3 for HCS and HCMS samples, respectively. The shapes of specimens after demolding are shown in Fig. 3c, while the sample compositions and designations are summarised in Table 3.

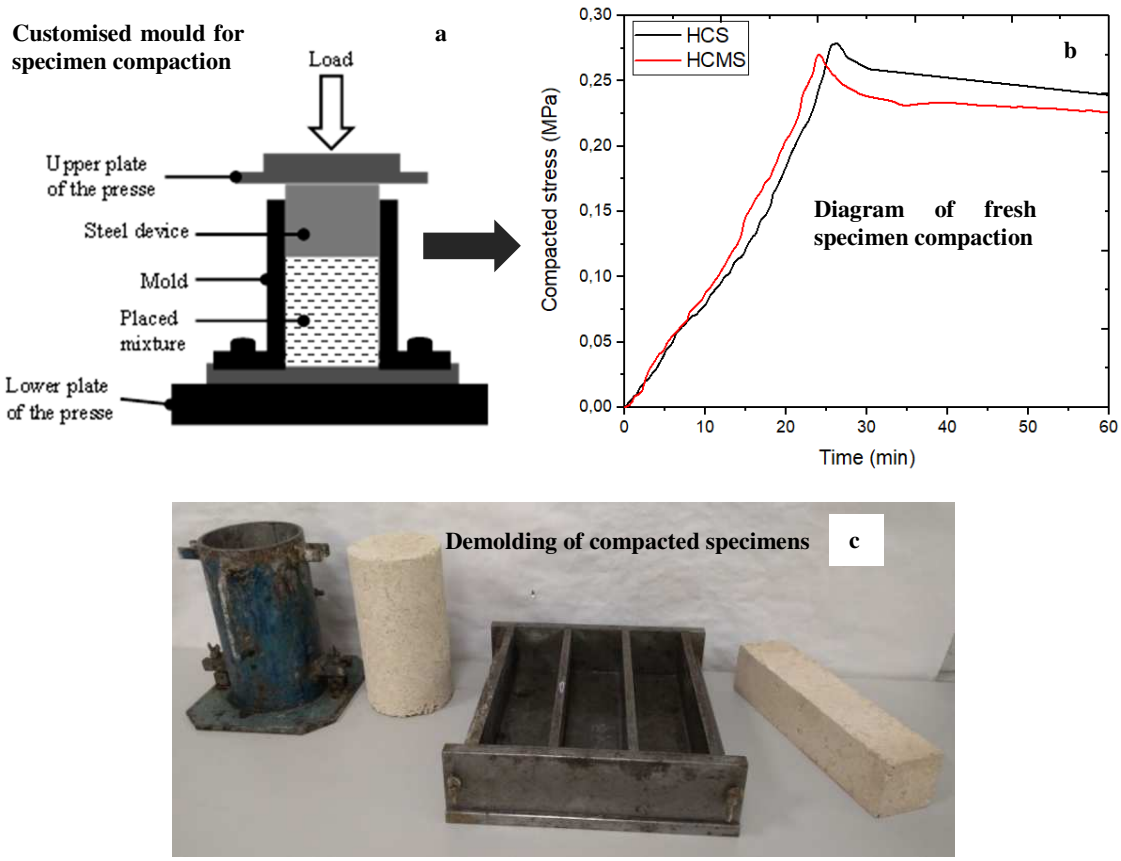

Fig. 3. Experimental set-up and casting process of specimens

Table 3

Composition mix and I.D of specimens

Sample-Mix ID	Tradical PF70 (kg/m^3)	Metakaolin (kg/m^3)	Hemp particles (kg/m^3)	Water (l/m^3)
HCS	180	0	52.5	250
HCMS	144	20	52.5	250

2.2 *Experimental testing and methods*

2.2.1 Accelerated wetting/drying aging test

There is currently no standard test to assess the resistance of hemp concrete to wetting and drying exposure. The specimens were subjected to fifty cycles and tested for their respective physico-mechanical properties for aging conditions of 0 (28-day control conditions), 15, 25, and 50 wetting/drying cycles. For all cycles, the samples were alternatively stored in a water container at 20 ± 2° C and then dried in the drying oven at 80 ± 2 °C (Fig. 4a). In order to establish the duration period of wetting and drying cycle, the mass change of specimens was measured at time intervals until reaching a constant value. Fig. 4b shows the hysteresis mass change of HCS and HCMS samples vs. time in wetting/drying phases, respectively, while a corresponding duration of 45 h immersion in tap water and 75 h drying in an oven, for each cycle, was established.

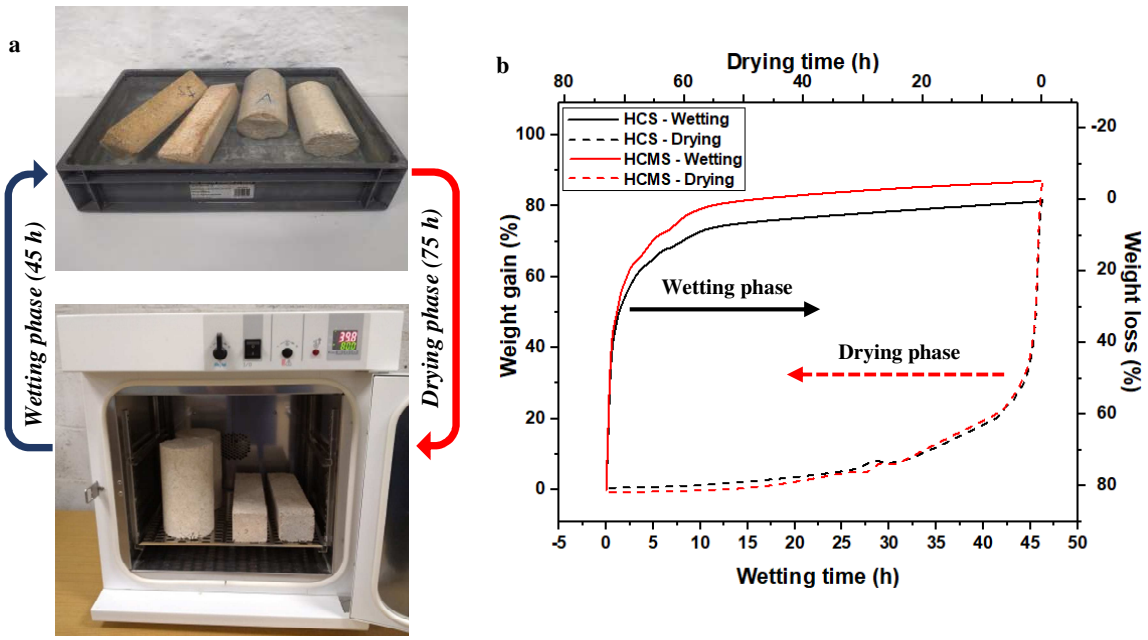

Fig. 4. Set up and duration test of wetting/drying cycle

2.2.2 Physical characterisation

The degradation level of specimens has been assessed by means of the variation in physical and mechanical properties, along the cycle intervals. The variation of mass loss was studied by weighing cylindrical (110 × 220 mm) specimen at the end of the drying phase of the cycle.

The vacuum saturation procedure has been used to measure the open porosity on prismatic (70 × 70 × 50 mm) specimen recovered after flexural testing, according to Standard ASTM C20 –00 [49]. Before testing, triplicate prismatic specimens were dried in an oven at 70 °C and then placed in a vacuum desiccator. To expel out initial trapped air in the pores of the specimen, the desiccator was connected to the vacuum pump which runs for 24 h at a pressure of 80 kPa. After weighing, the samples were soaked in another desiccator containing water,

while a vacuum pump still running. The mass of specimens was measured at time intervals until to reach full saturation. The corresponding open porosity was calculated following Eq. 3.

$$\phi_P = 100. \frac{M_{sat} - M_{dry}}{M_{sat} - M_{hyd}} \quad (3)$$

Where: ϕ_P (%) is the open porosity; M_{dry}, M_{sat}, and M_{hyd} (kg) are the dry mass, saturated mass, and hydrostatic mass of the specimen, respectively.

2.2.3. Mechanical characterisation

The characterisation of mechanical properties including compressive and flexural strengths was carried out on cylindrical and prismatic specimens, respectively, using an electromechanical testing machine SHIMADZU AG-IC model with a maximum load capacity of 250 kN (Fig. 5). The tests were conducted under loading rates of 4 mm/min and 0.8 mm/min, respectively, in accordance with European Standard EN 196-1 [50]. Both stress strain (in compression) and load displacement (in flexion) curves were recorded to evaluate several parameters such as compressive strength and corresponding ultimate strain, elastic modulus, and compressive toughness of the specimens at different aging cycles. In the same manner, the change in flexural strength and ultimate deflection, elastic stiffness, flexural modulus, and flexural toughness, were also reported. The compressive and flexural toughness was obtained by calculating the area under load–deflection curves up to ultimate deflection value.

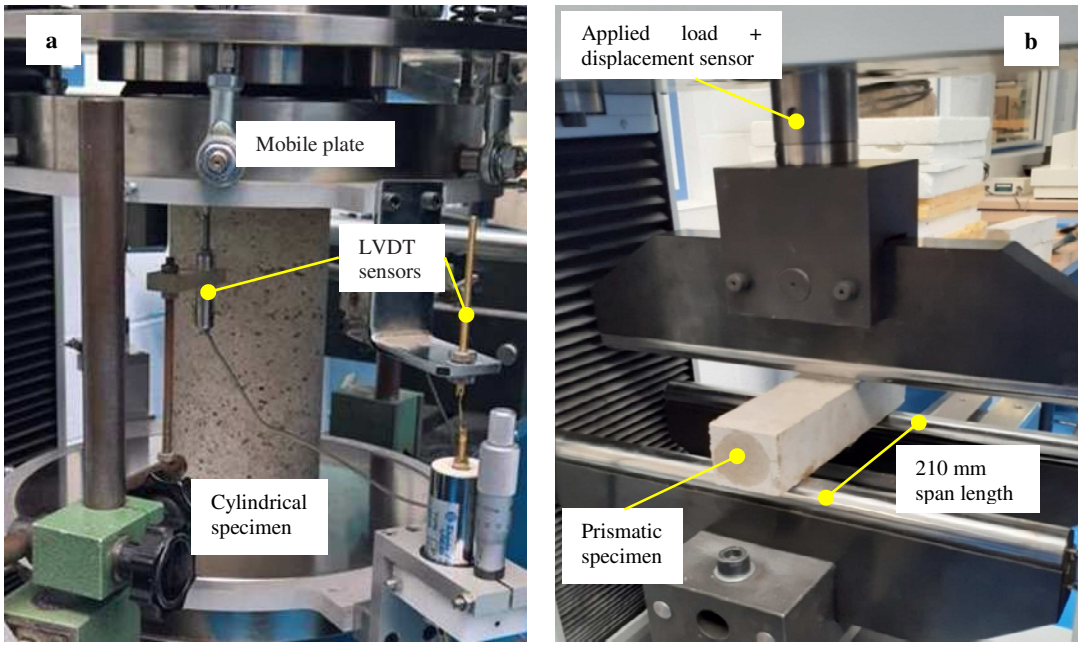

Fig. 5. Compressive (a) and three-point bending (b) tests of specimens

2.2.4 Embedded hemp particle characterisation

The degradation of the specimens was investigated by examining the deterioration degree of the embedded hemp particles. The properties investigated include morphological and mineralogical changes, and the variation

of crystallinity degree of hemp particles at cycle intervals. To perform these investigations, embedded hemp particles were pulled out from the specimens (with and without metakaolin) at aging cycle intervals and then brushed and rinsed with distilled water to remove the rest of the hydrate component deposits. Micro-analysis including SEM micrograph observations, thermogravimetric (TGA) and derived (DTG), and crystalline properties were investigated.

The microstructure analysis was performed on a FEI Quanta 200 Scanning Electron Microscope. The SEM analyses were conducted at low vacuum scanning conditions with an accelerating voltage ranging from 5 kV to 10 kV. Thermogravimetric (TGA) and derived (DTG) analyses were carried out using NETZSCH STA 449C thermal analyser at a heating rate of 10 °C/min, under a temperature ranged from 25 to 600 °C in air-atmosphere.

The crystalline properties, including percentage of crystallinity *Cr* (%) and crystallinity index *Cr. I*, of hemp particles embedded in HCS and HCMS specimens were investigated at different stages of aging cycles through X-ray diffraction (XRD). The analyses were performed on ground powders with an X_2 Scintag X-ray diffractometer in a θ-2θ configuration using CuKα source (λ= 1.54 Å) at - 40 kV and 35 mA, with step size of 0.02 (2 θ). The particles were scanned in step mode with a size of 0.02° (2 θ) in the angular range of 10 – 45 °, with 2°/min in a scanning speed. The percentage of crystallinity and crystallinity index were calculated from the X-ray diffraction spectra, using peak height method, according to Eq. 4 and Eq. 5 [51, 52].

$$Cr\ (\%) = \frac{I_{002}}{I_{002} + I_{am}} .100 \qquad (4)$$

$$Cr.I = \frac{I_{002} - I_{am}}{I_{002}} \qquad (5)$$

Where, I_{002} is the ultimate intensity diffraction of (002) lattice peak at 2 θ = 22.5 °, representing both crystalline and amorphous phases. I_{am} is the intensity of diffraction contributing to the amorphous amount, which is taken at a 2 θ angle between 18° and 19°, where the intensity is a minimum.

The high alkalinity of the pore solution of specimen is considered to be the main cause accelerating the degradation of cellulosic components. The variation of the alkalinity of specimens exposed to wetting/drying cycles was assessed through the measurement of their pore solutions using the suspension method, as described in several works [53, 54]. After mechanical testing of samples at different cycle intervals, 100 g of contained binder was taken from the specimen matrix and then manually separated from the embedded hemp particles. The obtained aggregates were crushed and sieved to 2/5 mm in size, before being mixed and continuously stirred with distilled water for 24 hours. Before pH measurements, the aqueous solution was vacuuming filtered using filter paper with 20 µm of pore size and centrifuged to remove the rest of suspended particles. The pore solution preparation of the sample and the pH-meter device HANNA edge HI-2004 02 are shown in Fig. 6.

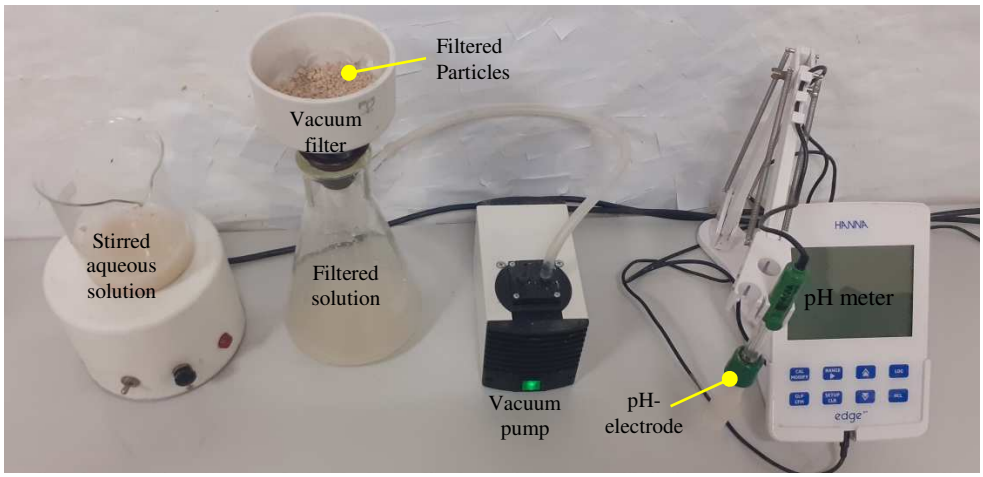

Fig. 6. Pore solution preparation of sample and pH-measurement set up

3 Results and discussion

3.1 Physical properties of specimens subjected to wetting/drying cycles

The results of the corresponding mass loss of samples, measured before being subjected to mechanical tests, are shown in Fig. 7a. It can be observed that there is no significant difference between HCS and HCMS specimens, during the first 25 testing cycles, with mass loss values ranging from 7.1% to 8.2%. For wetting/drying conditions above 25 cycles, a significant mass loss was observed for HCS, compared to the HCMS specimens. For 50 testing cycles, the mass loss values yielded were 12.2% and 8.4%, respectively. It is concluded that the protective effect of the metakaolin pozzolanic reaction carried out increases the cohesion of the matrix thus inducing less degradation of HCMS sample, compared to the HCS specimen.

The change in the open porosity has been also investigated as a critical factor leading to affect the strengthening of specimens under cyclic wetting and drying environment. As indicated in Fig. 7b, HCS specimen exhibited the highest open porosity, compared to the HCMS sample, with the correspondent values of 78% and 61%, respectively, for 50 aging cycles. The results also indicated that no appreciable difference in the porosity of the samples was observed for cycles less than 25. However, the highest difference between HCS and HCMS specimens was observed from the 25th cycle, thus highlighting the dilution effect of additional pozzolanic reaction between calcium hydroxide and silica which produced additional C-S-H crystals filled pores. These results agree with that obtained by Singh Gill et *al.* [55] in their research work using self-compacting concrete based on metakaolin and rice husk ash. According to the results, the pozzolanic reaction taking place should contribute towards durability of the hemp concrete by enhancing binder strength level which results in a high bond strength between hemp particles and matrix. These results agree with those obtained by Walker et *al.* [12] which indicated that the addition of natural pozzolans with a high reactivity to the commercial lime binder (NHL 3.5) results in an increase of compressive strength due to the reduction of the porosity in the matrix.

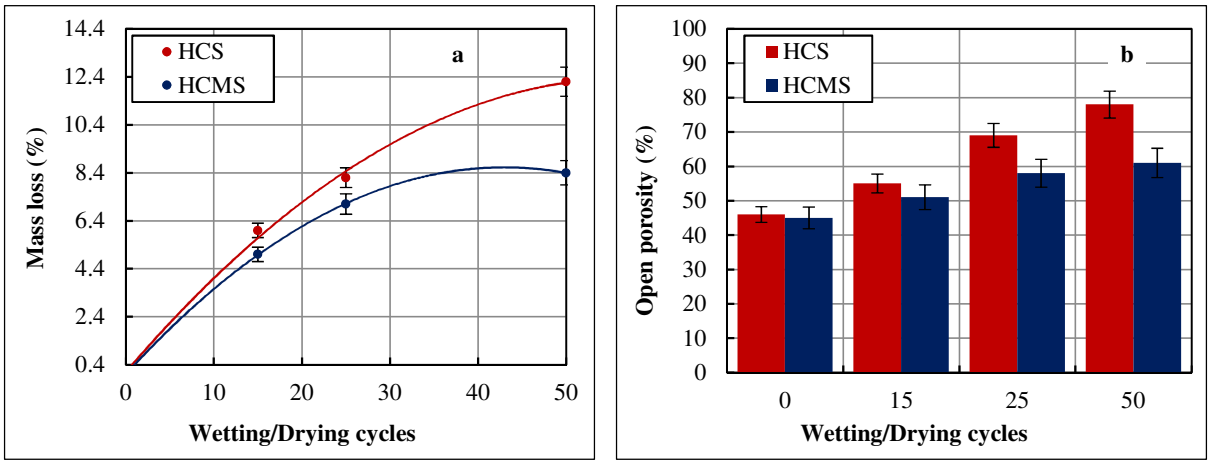

Fig. 7. Variation of physical properties of specimens vs. aging cycles. (a): Mass loss; (b): Open porosity

3.2 Mechanical properties of specimens under wetting/drying cycles

3.2.1 Compressive strength change of hemp concrete

The typical compressive stress-strain diagrams of HCS and HCMS specimens after 0, 15, 25, and 50 of wetting and drying cycles are shown in Fig. 8a and Fig. 8b, respectively. The corresponding average mechanical parameter values derived from the tests, including compressive strength, ultimate strain, elastic modulus, and compressive toughness energy are listed in Table 4. After 50 cycles of aging, the compressive strength decreased from 1.45 to 0.20 MPa, and from 1.35 to 0.35 MPa, respectively, while the corresponding decrease levels of 86.2% and 73.3% make the HCMS specimen more durable than HCS sample. It can be observed that prior to cyclic aging, the specimen containing metakaolin exhibited lower compressive strength than the HCS sample, which in contrast, becomes higher after 15 wetting/drying cycles. This difference is may be due to progressive additional hydration taking place during the wetting phase, thus enhancing the amount of C-S-H crystals resulting from pozzolanic reaction in the HCMS matrix. It is well known that the pozzolanic reaction tends to strengthen more slowly than the reaction of lime binder [56]. Fig. 9a shows the SEM observations of specimen microstructures which indicated abundant free Ca $(OH)_2$ hydrates as needle-shaped for Tradical binder matrix. In contrast, the pozzolanic binder is largely hydrated to produce a high amount of C-H-S hydrates (Fig. 9b). In addition, the retained water by hemp particles during the wetting phase could contribute to enhancing the pozzolanic reactivity particularly at hemp particle/binder interfacial zone. These results agree with those obtained by R. Walker et *al*. [12], which have shown the effectiveness of retained water by vegetable particles in improving the pozzolanic hydration in vegetable concrete. However, the higher reduction in compressive strength for HCS sample, compared to the HCMS specimen, is also due to the more bond strength of hemp particles to the matrix with pozzolane material. The reduction in compressive strength is related to the bond defect of hemp particles to the matrix, as the aging test continues, due to their alternative swelling and shrinking

under cyclic wetting and drying effect. This results in the debonding of particles from the binder thus allowing increasing the porosity in the matrix. As the mass loss result, the reduction in mechanical performances of sample is due to the weakening of the Interfacial Transition Zone (ITZ) that favors the propagation of cracks in the matrix. In terms of bonding, the SEM micrographs of ITZ surface of particles/matrix, after 50 wetting/drying cycles, are reported in Fig. 10. The hemp particles/matrix bond appears to be lower for HCS sample, in contrast to that observed for HCMS specimen, where the layer deposits of pozzolanic hydrates on the surface of hemp particles favors their adherence to the binder matrix. The compressive strength defect could also be related to the change in the morphological properties and the internal damages of embedded hemp particles with continuous aging cycles, due to their high water sensitivity. This point should be addressed in the next section.

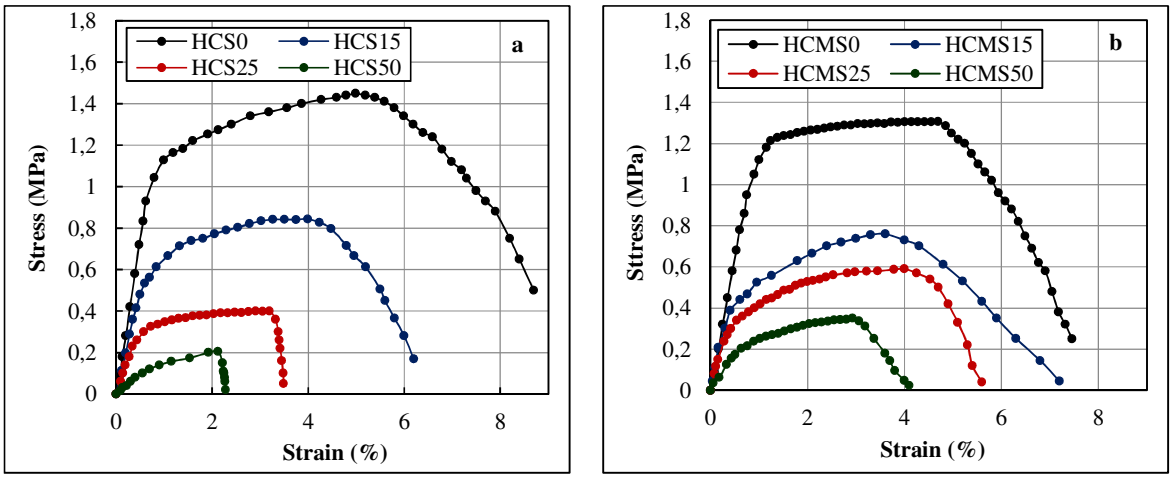

Fig. 8. Typical stress-strain diagrams of HCS (a) and HCMS (b) samples vs. wetting/drying cycles

Table 4

Mechanical properties of specimens submitted to compressive test, at different aging stages

Aging cycle	Compressive strength (MPa)		Ultimate strain (%)		Elastic modulus (MPa)		Compressive toughness (J)	
	HCS	***HCMS***	***HCS***	***HCMS***	***HCS***	***HCMS***	***HCS***	***HCMS***
0	1.45 ±0.2	1.35 ±0.3	5.00 ±0.5	4.73 ±0.2	145 ±10	128 ±12	124.96 ±10	118.56 ±10
15	0.85 ±0.1	0.76 ±0.2	3.96 ±0.5	3.60 ±0.4	95 ±12	98 ±10	53.00 ±15	50.60 ±12
25	0.40 ±0.1	0.60 ±0.2	3.34 ±0.6	4.00 ±0.4	60 ±10	79 ±8	22.63 ±5	37.61 ±10
50	0.20 ±0.08	0.35 ±0.1	2.08 ±0.7	2.95 ±0.3	19 ±10	40 ±5	5.96 ±6	16.09 ±6

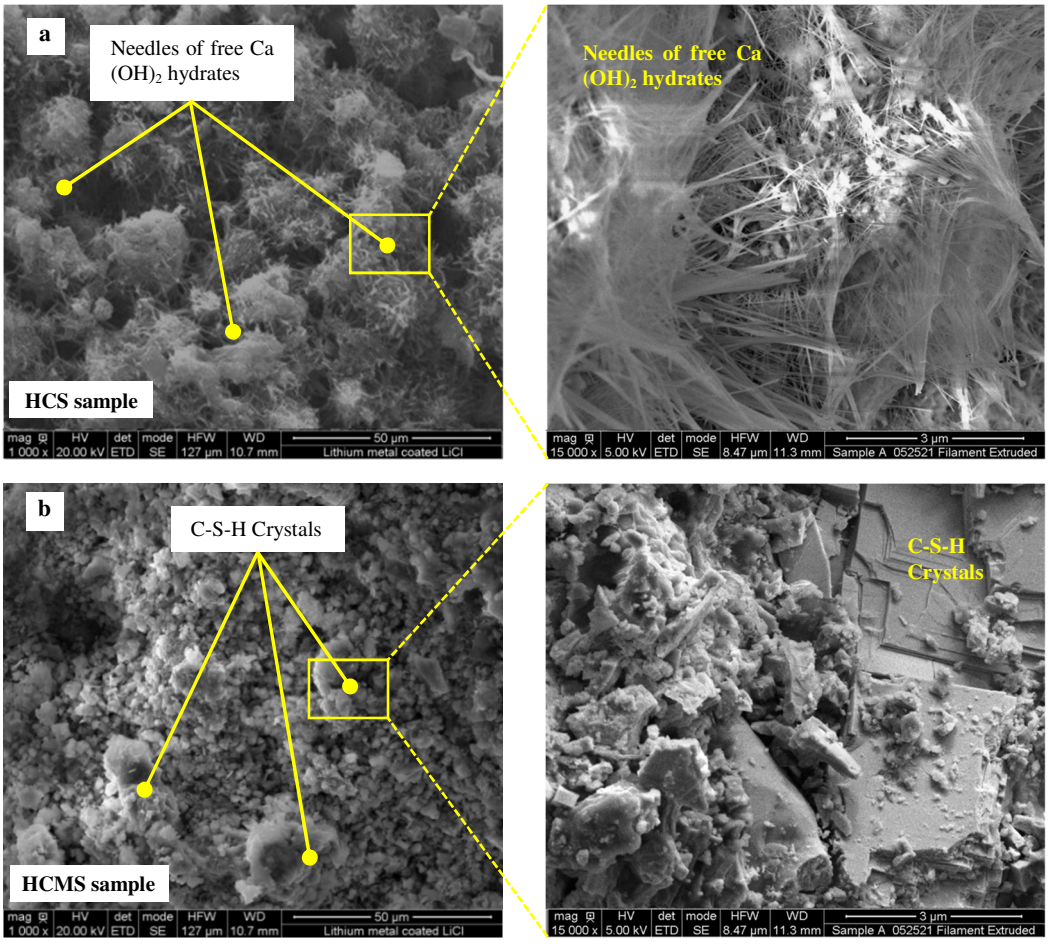

Fig. 9. SEM micrographs of hydration products of specimens after 15 wetting/drying cycles

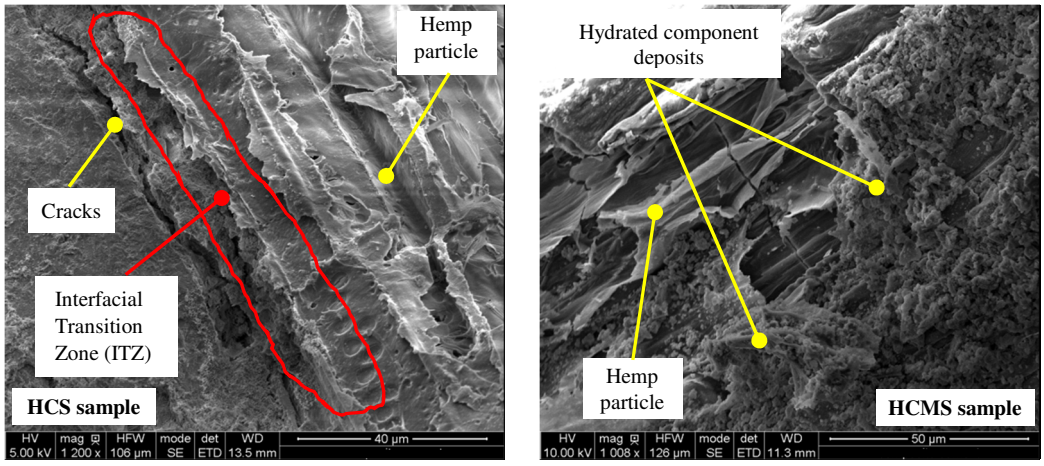

Fig. 10. SEM micrographs of hemp particle matrix bonding, after 50 wetting/drying cycles

3.2.2 Elasticity behavior change of hemp concrete

The degradation of hemp concrete specimen was also evaluated by examining the variation of several mechanical parameters derived from compressive tests. As can be observed in Table 4, the increase in aging cycles leads to decrease the strain capacity of specimens at failure, where the value varied from 5% to 2.08% and from 4.75% to 2.95%, for HCS and HCMS specimens, respectively. Overall, before aging, the specimens

exhibited ductile behavior evidenced by higher deformation ability, where the ultimate strain values are in the same order, without significant effect of metakaolin addition. After 50 cycles, HCMS specimen exhibited 28.2% greater strain capacity than of HCS sample. The effectiveness of metakaolin was also observed as HCMS specimen yields the greater elastic modulus and the best compressive toughness energy, which are 110.5% and 170.2% higher than those obtained for HCS sample, respectively (see Table 4). It is concluded that the combination of metakaolin and Tradical binder which leads to better bond strength of hemp particles to the matrix, through the additional production of C-S-H gel, is the main reason for the better durability of HCMS specimen. However, the deterioration level of embedded hemp particles may also be effective in the degradation mechanism of concrete sample.

The positive effect of metakaolin addition to make the specimen more durable was also observed from its post-cracking behavior. Fig. 11 indicated that although strain capacity decreases along aging cycles, HCMS specimen exhibited more post-cracking toughness than HCS sample. For 50 cycles, the corresponding values varied from 211.30 J to 6.45 J and 198 J to 25.67 J, for HCS and HCMS specimens, respectively. In contrast to the brittle failure observed for HCS sample, where the post-cracking phase is almost non-existent, a controlled load decrease was noticed for HCMS specimen mainly attributed to the more bond of hemp particles and their lower degradation. Fig. 12 shows the shapes of typical failure for specimens submitted to compressive test after 50 cycles, where HCS specimen undergoes a brittle failure characterised by a total fracture resulting in shattering into small pieces. In contrast, HCMS specimen experienced a ductile failure allowing to support loads after reaching its maximum capacity. The applied load is transferred and distributed along the hemp particles/matrix interface without disintegration of specimens due to the bridging action of cracks. It results that the tension cracks become narrower and shorter in specimens. A similar trend has been observed by several authors when vegetable materials were used as additives in concrete based on different binder types [57, 58].

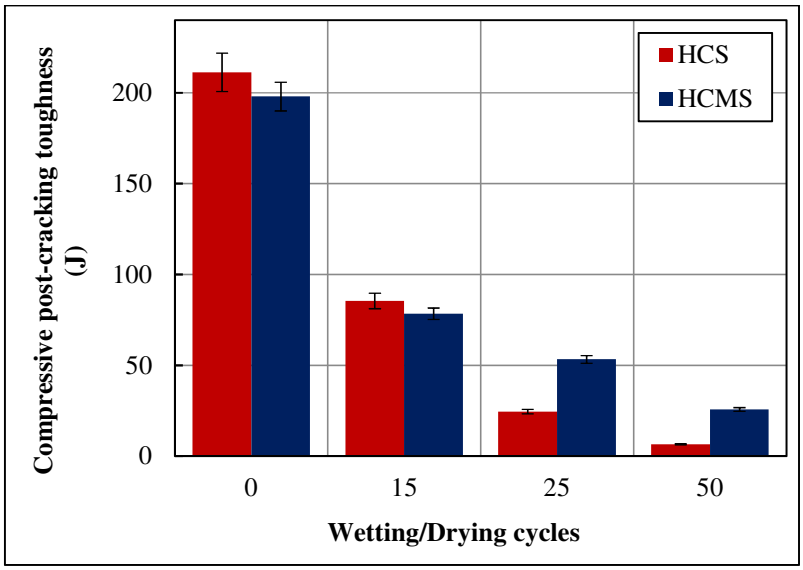

Fig. 11. Post-cracking toughness of specimens under compressive test vs. wetting/drying cycles

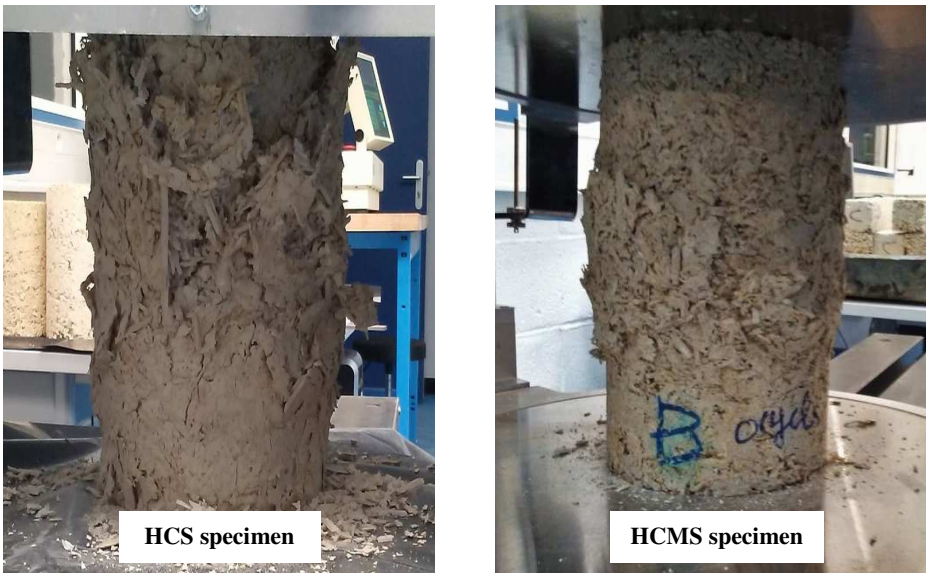

Fig. 12. Shapes of specimens submitted to compressive test, after 50 aging cycles

3.2.3 Flexural strength change of hemp concrete

Fig. 13 illustrates typical load-deflection curves of specimens subjected to continuous wetting and drying cycles, while the corresponding parameter values are listed in Table 5. Similarly to compressive-test response, the degradation of the specimen is evidenced by the decrease in maximum sustained load to reach failure, where the corresponding flexural strength was decreased from 1.78 to 0.22 MPa and from 1.64 to 0.56 MPa, for HCS and HCMS specimens, respectively. The hemp particle-matrix interfacial zone strength level is considered to be the predominant parameter which governs the failure of the specimen. Similar trend can also be observed for corresponding deflection at failure, after 50 aging cycles, which declined by 84.5% and 44.6%, respectively. However, the progressive decrease of the slope in elastic region of the load-deflection curve indicates that the

wetting and drying cycle action result a more brittleness of HCS sample than HCMS specimen, where the reduction of the corresponding elastic modulus rate is 61.71% and 38.8%, respectively. Furthermore, the reduction of the binder porosity due to the increase of pozzolanic products thereby minimise vulnerability of specimens under action of wetting-drying cycles.

Flexural toughness variation is one of the most important performance indicators of energy absorption ability for specimens with continuous aging cycles. As shown in Fig. 14, the decline in post-cracking toughness is directly related to the binder type, where a more severe degradation of HCS specimen is observed as evidenced by a significant decrease in toughness value. For 50 aging cycles, the corresponding toughness decreases are 98.5% and 81%, for HCS and HCMS, respectively. However, the progressive disappearance of post-cracking phase, with continuous aging cycles, resulted from increasing of HCS specimen brittleness, whereas HCMS specimen containing metakaolin exhibited ductile behavior. This results that after ultimate strength, the cracks cannot propagate without stretching and debonding of the hemp particles, thus allowing to absorb a large additional amount of energy. This behavior is related to the low degradation of hemp particles evidenced by their ability to bridge and arrest the cracks within the interfacial zone. It is concluded that the combination of metakaolin and Tradical PF70-binder leads to make the hemp concrete less sensitive to wetting and drying cycles.

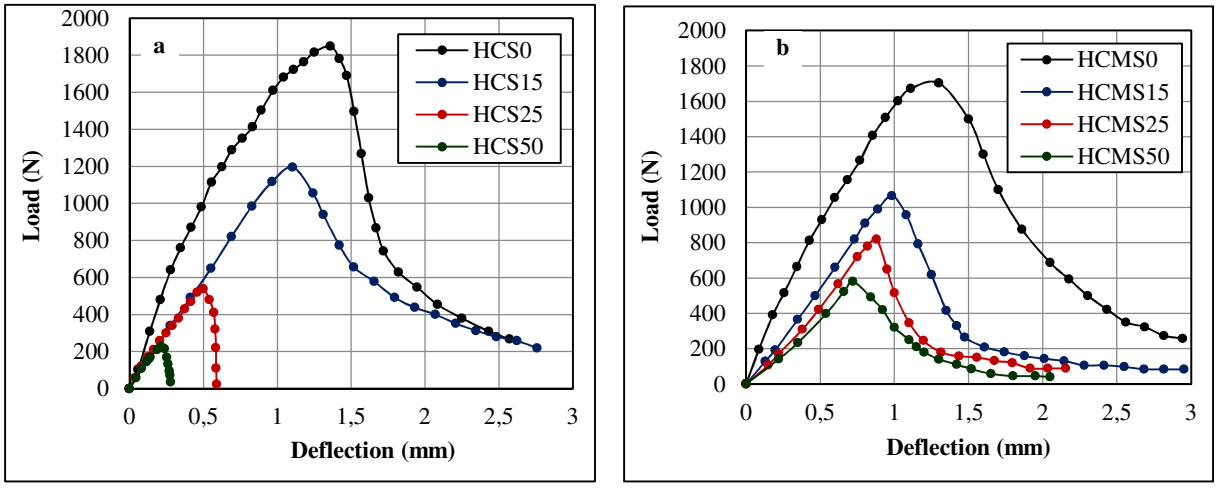

Fig. 13. Typical load-deflection curves of HCS (a) and HCMS (b) samples vs. wetting/drying cycles

Table 5

Mechanical properties of specimens submitted to tree point bending test, at different aging cycles

Aging cycle	Flexural strength (MPa)		Ultimate deflection (mm)		Elastic modulus (MPa)		Post-cracking toughness (J)	
	HCS	***HCMS***	***HCS***	***HCMS***	***HCS***	***HCMS***	***HCS***	***HCMS***
0	1.78 ±0.1	1.64 (0.3	1.36 ±0.1	1.30 ±0.2	7.00 ±0.6	6.28 ±0.7	2.65 ±0.5	2.52 ±0.3
15	1.15 ±0.1	1.02 ±0.1	1.10 ±0.05	0.98 ±0.05	4.25 ±0.5	3.96 ±0.5	1.59 ±0.1	1.48 ±0.4
25	0.52 ±0.05	0.79 ±0.06	0.50 ±0.08	0.86 ±0.06	3.29 ±0.2	4.67 ±0.6	0.19 ±0.08	0.62 ±0.2
50	0.22 ±0.04	0.56 ±0.02	0.21 ±0.02	0.72 ±0.05	2.68 ±0.3	3.84 ±0.4	0.04 ±0.01	0.48 ±0.1

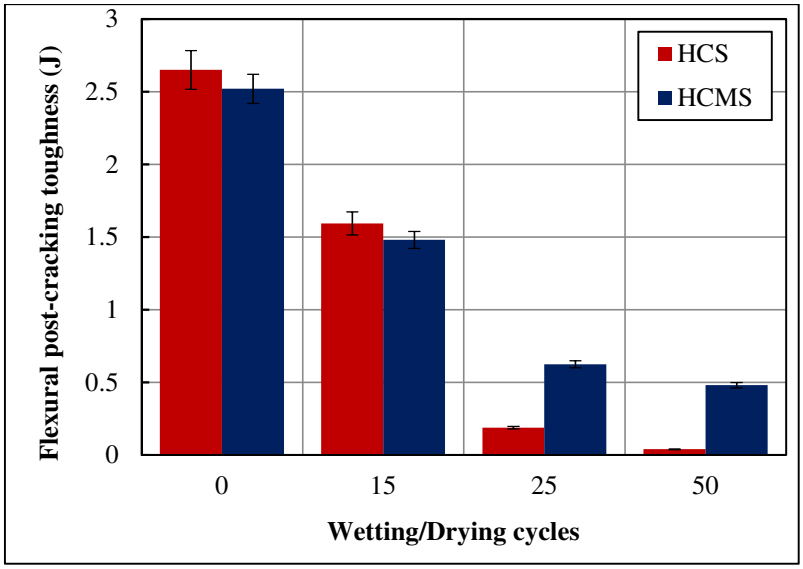

Fig. 14. Post-cracking toughness of specimens under tree point bending test vs. wetting/drying cycles

3.3 Degradation of embedded hemp particles in the binder matrix of concretes

3.3.1 Thermal analysis

Beside the loss of physico-mechanical properties of hemp concrete subjected to wetting and drying cycles, the degradation of embedded hemp particle is considered to be one of the main indicators contributing to the concrete specimen deterioration. The degradation of embedded hemp particles was investigated by analysing several parameters like their residual cellulosic components, surface morphology modifications, and the change of the crystalline properties at 0, 25 and 50 wetting and drying cycles. To perform these analyses, the embedded hemp particles were pulled out from the matrixes of HCS and HCMS specimens at aging cycle intervals and then brushed and rinsed with distilled water to remove the rest of the hydrate deposits. Before being analysed, the hemp shivs were crushed at fine particles and then submitted to thermal analyses. According to several author's

research, the degradation of vegetable particles is characterised by the dissolution of main components like lignin and hemicellulose, and alkaline hydrolysis of cellulose constituent [59, 60].

The thermal decomposition process of embedded hemp particles in the form of TGA and derived DTG curves, are shown in Fig. 15, while the residual cellulosic components are listed in Table 6. As shown in Fig. 15a and Fig. 15c, several degradation stages are related to the presence of different components that are characterised by different temperature ranges of decomposition. The corresponding peaks illustrated in Fig. 15b and Fig. 15d are referred to the decomposition of hemicellulose and the main part of lignin, and the cellulose, respectively [61]. The first step displayed by the TGA curve, followed by the thermal stability (step 2), corresponds to both the water evaporation and the decomposition of impurities substances. The step 3 corresponds to the lignin and hemicellulose decomposition for temperature ranges from 230 to 370 °C, while the hemp embedded in HCMS matrix exhibited the lower degradation grade. After 50 aging cycles, the corresponding decrease levels of (lignin + hemicellulose) yielded 50.86% and 29.87% for HCS and HCMS samples, respectively. These results highlighted the effectiveness of additional development of pozzolanic hydrates, which serve as a protective barrier at interfacial zone around the hemp particles against physical degradations. The dissolution of lignin and hemicellulose induced the stripping of cellulose mico-fibrils contained in hemp particles, due to the deterioration of amorphous regions in cellulose chains of particles. The corresponding residual cellulosic components of embedded hemp particles in different specimens are shown in Fig. 16.

The obtained mass loss in the TGA curve occurred for temperature ranges from 370 to 500 °C corresponds to the decomposition of cellulose component, as observed (step 4). After 50 aging cycles, the embedded hemp particles encounter cellulose content losses of 62.31% and 40.15% for HCS and HCMS samples, respectively. These results highlighted the efficiency of metakaolin addition to make the hemp particles less vulnerable under the action of wetting-drying cycle, by reducing the alkalinity of the pore solution in the binder matrix. According to several research works, the highly alkaline pore solution rich in free Ca^{2+} ions from the soluble calcium hydroxide components is well known to be the major cause of vegetable particles degradation. This mineral-rich fluid can infiltrate into the hemp particle and degrades the cellulose molecules [51, 62]. The lower degradation of cellulose in hemp particles from HCMS specimen results to the consumption of calcium hydroxide by the pozzolanic reaction, which gives rise to reduce the alkalinity of the matrix medium. The reaction occurred between the calcium ions and the amorphous silica, produce stable components of C-S-H, according to the reaction mechanism:

$$3Ca^{++} + 2H_2SiO_4^{2-} + 2OH^- + 2H_2O \longrightarrow Ca_3[H_2Si_2O_7](OH)_2 . 3H_2O$$

For temperature range from 500 to 600 °C (step 5), the additional mass loss corresponds to the decomposition of non-organic components such as calcium hydroxide which precipitated in cell walls of embedded hemp particles. As shown in Table 6, the highest mass loss value, corresponding mainly to the amount of Ca^{2+} ion deposits, was occurred with embedded hemp particles in Trdical PF70-based binder than the binder containing metakaolin. This indicates that hemp particles encounter the most severe alkaline attack with Tradical PF70-based lime binder medium due to its high degree of alkalinity.

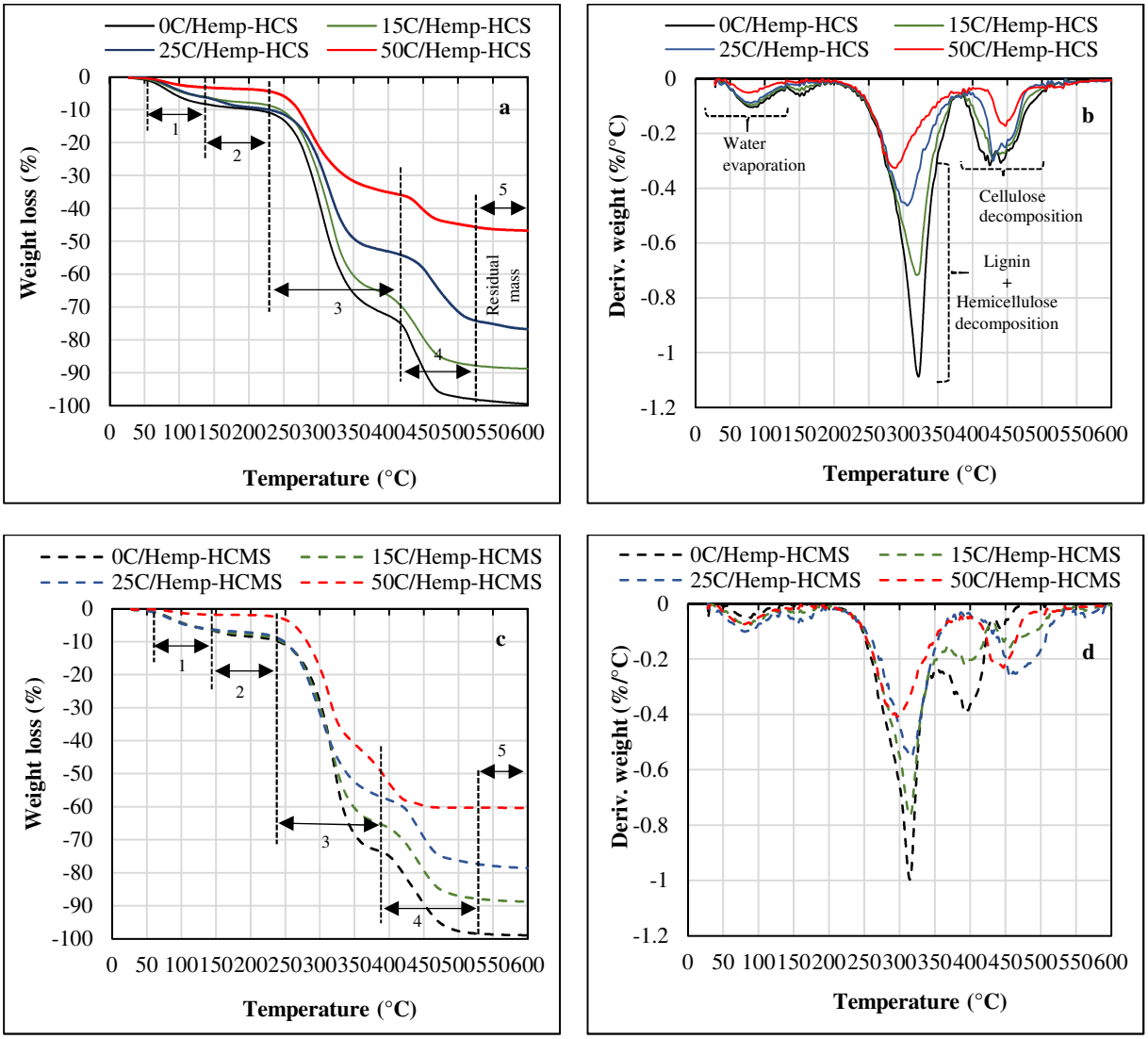

Fig. 15. TGA (a) and derived DTG (b) curves of embedded hemp in HCS (a, b) and HCMS (c, d) specimens

Table 6

Mass loss of embedded hemp particle in HCS and HCMS samples by thermogravimetric analysis at different aging cycles

Hemp particle & ID	Mass loss (%) in each step (for different temperature ranges)				
	Step 1	Step 2	Step 3[1]	Step 4[2]	Step 5[3]

	(50 - 130 °C)	(130 - 230 °C)	(230 - 370 °C)	(370 - 500 °C)	(> 500 °C)
0C/Hemp-HCS[a]	6.1 ±0.5	Thermal stability	63.3 (2	25.2 ±3	1.9 ±0.5
15C/Hemp-HCS[a]	6.0 ±0.5		59.5 ±3	21.2 ±2	11.4 ±3
25C/Hemp-HCS[a]	6.3 ±0.7		45.3 ±4	19.4 ±2	25.2 ±3
50C/Hemp-HCS[a]	3.0 ±0.5		31.1 ±3	9.5 ±2	54.3 ±5
0C/Hemp-HCMS[b]	6.2 ±0.5		65.6 ±6	26.4 ±2	1.5 ±0.3
15C/Hemp-HCMS[b]	6.0 ±0.2		60.5 ±4	24.2 ±3	10.8 ±3
25C/Hemp-HCMS[b]	5.6 ±0.2		52.1 ±4	23,6 ±3	22.5 ±3
50C/Hemp-HCMS[b]	1.7 ±0.1		46.0 ±5	15.8 ±2	39.7 ±4

[1] (Lignin + Hemicellulose) decomposition; [2] (Cellulose) decomposition; [3] Residual mass (non-organic)

[a, b] Embedded hemp particle in HSC and HCMS samples, at 0, 15, 25, and 50 wetting/drying cycles

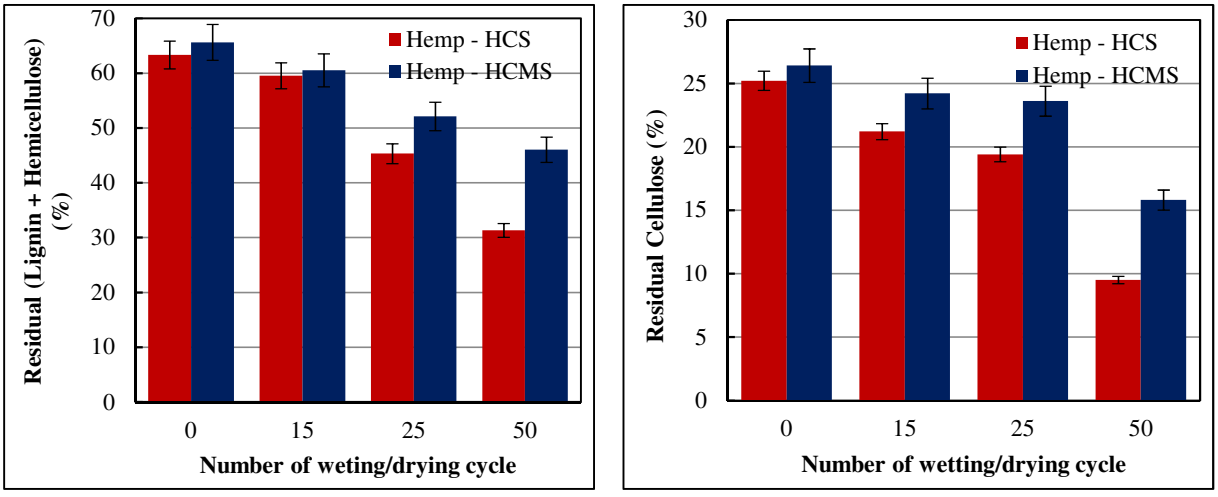

Fig. 16. Residual components of embedded hemp particles in different specimens vs. aging cycles

3.3.2 Microstructure analysis

A microstructure analysis was carried out on the longitudinal and cross sections of embedded hemp particles, to investigate their degradation degree under the effect of aging cycles. Fig. 17a and Fig. 17b show the modification surface morphology of particles after 15 aging cycles, while a deposition of hydration products mainly calcium hydroxide compounds, has been observed for embedded hemp in HCS matrix (15C/Hemp-HCS). For the hemp pull-out from HCMS specimen (15C/Hemp-HCMS), it can be seen that the surface morphology still remained intact without significant hydration component deposits. This difference is related to the local pozzolanic reaction occurred around the surface of the particles, which leads to consume calcium hydroxide components to produce C-S-H crystals. Fig. 17c and Fig. 17d indicated that after 50 cycles, the hemp particles embedded in HCS matrix (50C/Hemp-HCS) exhibit signs of mineralisation, evidenced by the high

scattered cellulose fibrils in the external wall. The severe hemp deterioration results from decomposition of amorphous components of lignin and hemicellulose, than the particle from HCMS matrix (50C/Hemp-HCMS) witch encounters slight attacks.

The SEM micrographs of hemp cross sections after 50 aging cycles have been compared in Fig. 17e and Fig. 17f. It can be observed that the cell walls of embedded hemp in HCS matrix (50C/Hemp-HCS) are mineralised due to the precipitation of Ca^{2+}, which results in a more serious damage of the internal cell wall structure, while the space of micro-fibrils is filled with hydration products, causing erosion of amorphous phase and embrittlement of hemp particles. The microstructure analyses of hemp from HCMS matrix (50C/hemp-HCMS) indicated a low alkaline attack degree of the amorphous phase, characterised by a slight defibrillation of cellulose micro-fibrils. Although a small amount of hydration product deposits has been observed, the integrity of the cell walls still remains intact without significant mineralisation. This results in the better interfacial adhesion of hemp to the matrix, thus increasing the residual mechanical performances of hemp concrete. These results showed the effectiveness of metakaolin addition to substantially mitigate degradation of embedded hemp in concrete specimen, by slowing their mineralisation through the reduction of the matrix alkalinity. The obtained results agree with that reported in several research works concerning the relationship between the dissolved calcium hydroxide and the alkalinity degree of hydraulic binder medium [32, 63].

The testing data of pH value of pore solutions from HCS and HCMS specimens along aging cycles has been measured and reported in Fig. 18. It can be observed that in HCS matrix (neat Tradical lime binder), the alkalinity of pore solution remained relatively stable with a pH-value varied from 13.6 to 13, after 50 aging cycles. For HCMS specimen, the partial replacement of lime binder by metakaolin appears to be an effective way to substantially reduce alkalinity degree, while the pH value decreased from 13.4 to 11.6. This may be due to the high binding of alkalis in the additional amounts of C-S-H produced by the pozzolanic reaction [60, 64, 65]. However, it's concluded that the incorporation of metakaolin mitigates the alkali degradation of hemp particles thus making hemp concrete more resistant under aging cycles.

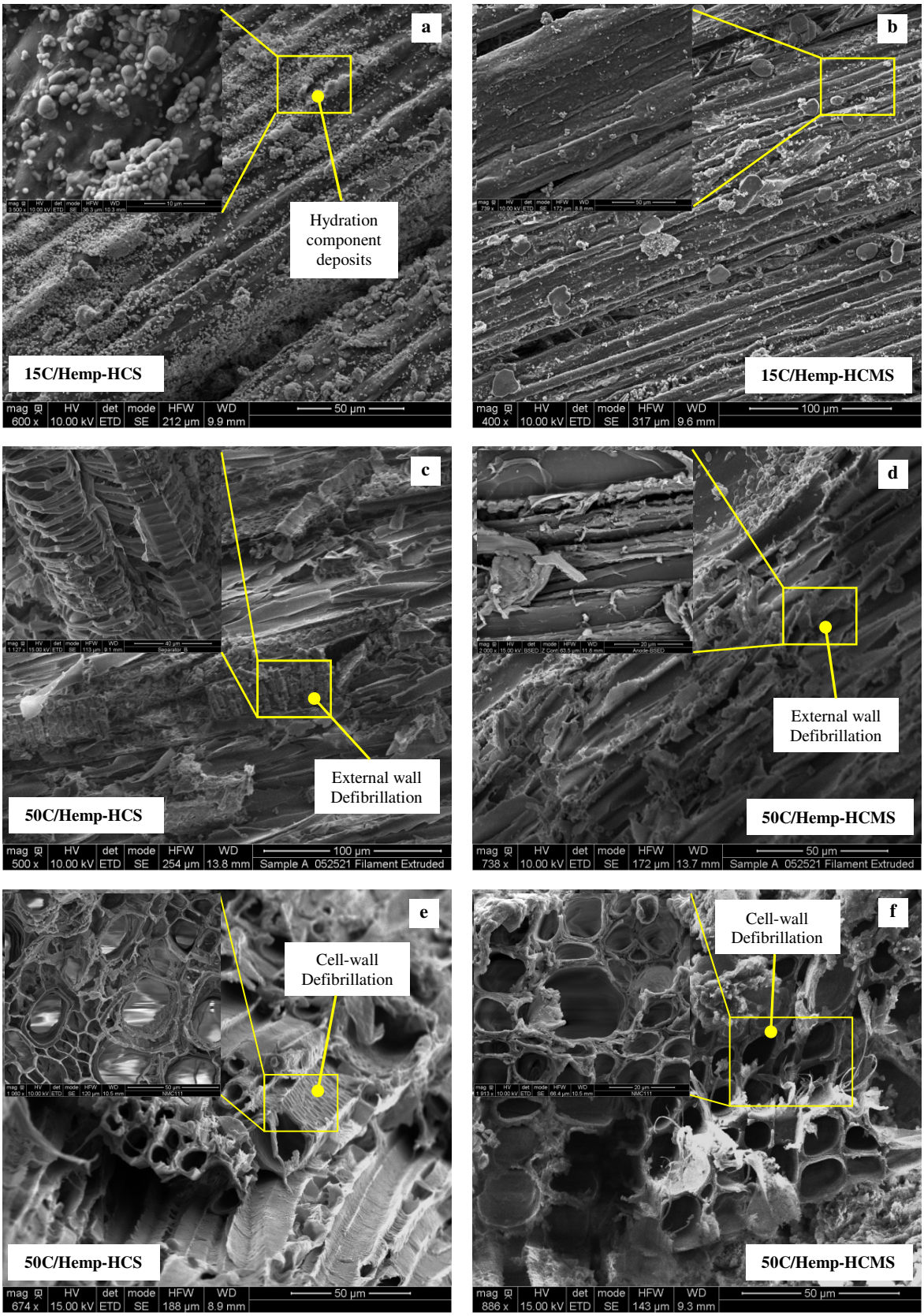

Fig. 17. SEM micrographs of embedded hemp particles in HCS and HCMS matrixes vs. wetting/drying cycles

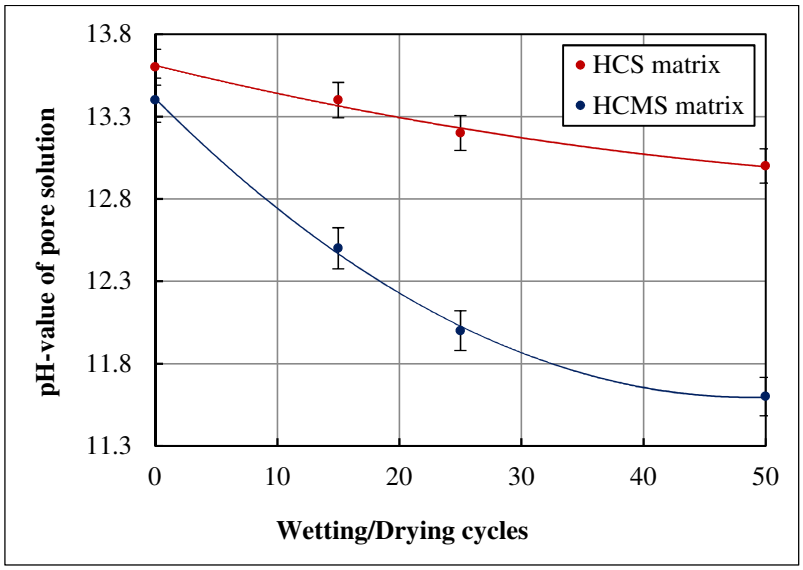

Fig. 18. Variation of pH value in pore solution of HCS and HCMS specimens vs. aging cycles

3.3.3 X-ray diffraction analysis

The degradation degree of hemp particles, due to a combination of mineralisation and alkaline attack mechanisms, could be analysed by quantifying their percentage of crystallinity (*Cr*) and the corresponding crystallinity index (*Cr. I*) [51, 52]. To perform crystalline property measurements, the XRD diffractograms of embedded hemp in HSC and HCMS specimens after 0, 15, 25, and 50 aging cycles, compared to the raw particles are depicted in Fig. 19, while the corresponding crystalline properties are listed in Table 7. It can be observed that the crystalline phase exhibited peak at 2 $\theta \approx 22.5°$ corresponding to (002) lattice plane. The peak extending from 17° to 19° corresponds to the (am) lattice planes of amorphous phase [51, 66].

The peaks of Ca $(OH)_2$ hydrates located at 25° and 31° intervals are present for all hemp particles from each concrete, while the intensive peak is found on that pulled out from the HCS sample. It can be observed that the peaks located around 33°, corresponding to the dominant peaks of C-S-H and $CaCO_3$ products, become higher for embedded hemp particles pulled out from HCMS specimen, after 50 cycles. This is caused by the pozzolanic reaction of metakaolin, which consumes hydroxide calcium to produce more C-S-H crystals.

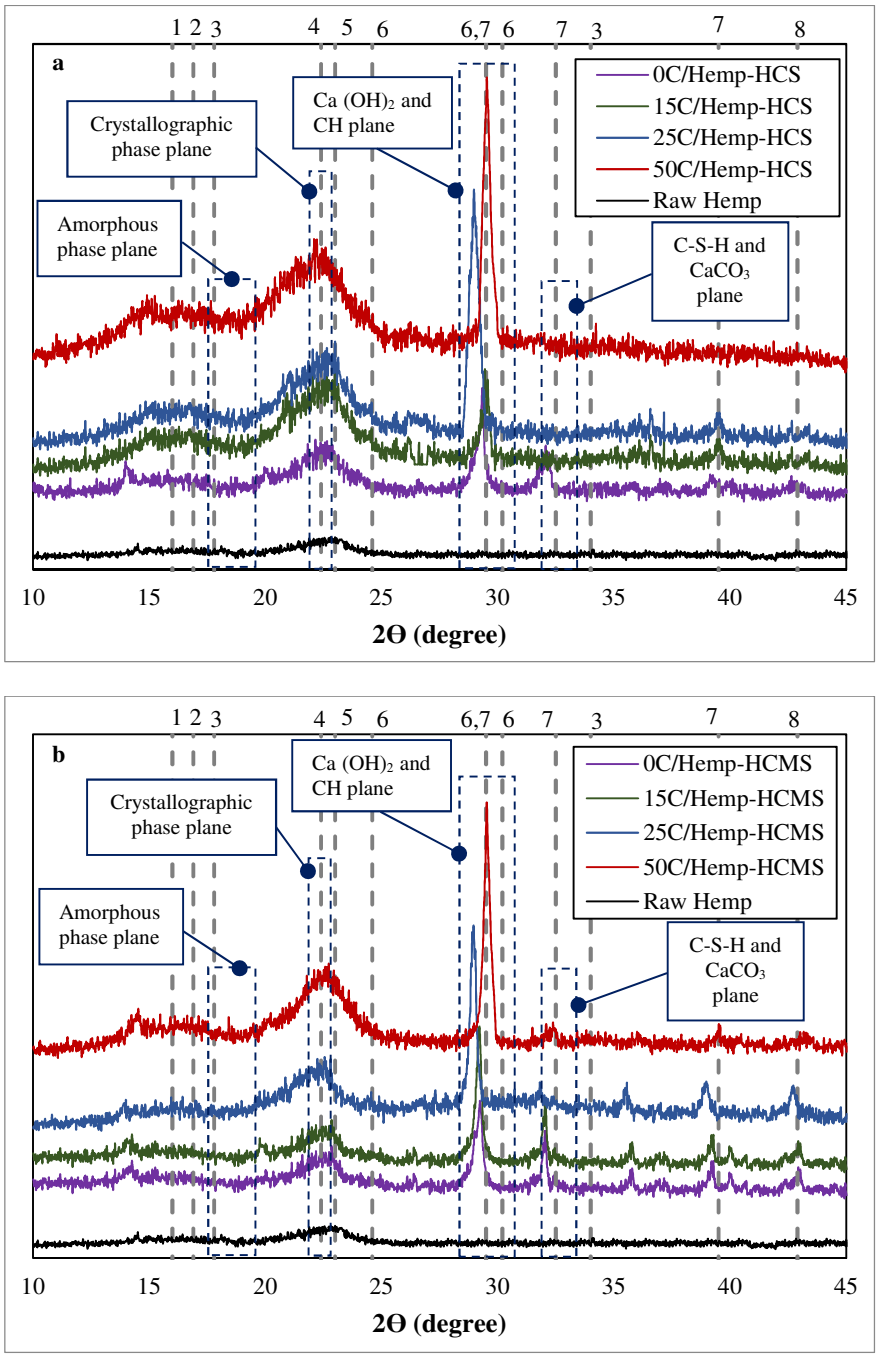

Fig. 19. XRD pattern of embedded hemp particles in HCS (a) and HCMS (b) vs. aging cycles

Table 7

Parameters of crystalline properties of embedded hemp particles during aging cycles

Hemp particle ID	Aging cycles	Peak position I_{am} (2 θ = 18° - 19°)	Peak position I_{002} (2 θ = 22°)	*Cr (%)*	*Cr. I*
Hemp/HCS matrix[1]	0	60.71 ±5	120.61 (10	66.52 ±3	0.49 ±0.08
	15	42.75 ±6	89.44 ±5	67.66 ±4	0.52 ±0.02
	25	66.07 ±5	142.32 ±6	68.30 ±3	0.53 ±0.02
	50	65.06 ±7	174.48 ±7	72.84 ±2	0.62 ±0.03
Hemp/HCMS matrix[2]	0	52.46 ±5	96.8 ±5	64.85 ±2	0.45 ±0.05
	15	101.96 ±4	206.4 ±10	66.93 ±3	0.50 ±0.04
	25	64.15 ±6	132.44 ±5	67.36 ±2	0.51 ±0.03
	50	56.76 ±5	121.32 ±6	68.13 ±2	0.53 ±0.02

The variation of percentage crystanillity (*Cr*) and crystallinity index (*Cr. I*) of embedded hemp particles in different specimens along aging cycles is depicted in Fig. 20. It should be noted that at every stage, the lowest crystalline properties were obtained for embedded hemp in HCMS matrix, compared to HCS specimen. At 50 wetting/drying cycles, the crystalline properties increased by 9.5% and 5.05% of *Cr*, and 26.53% and 17.77% of *Cr. I*, for hemp particles embedded in HCS and HCMS specimens, respectively. The use of metakaolin as a partial replacement of commercial lime binder appears to minimise the hemp particle degradation, as evidenced by the low increase in crystalline properties. Fig. 21 shows a strong dependence between the *Cr. I* and pH value of pore solution, while the matrix with low alkalinity induced a lower crystallinity degree of hemp particles. Fig. 21 also shows a notable decrease in the pH value when metakaolin was added, thus inducing a substantial enhancement of residual cellulose. These results agree with the mechanical tests data, as analysed above, which highlighted the effectiveness of metakaolin addition to enhance the durability of hemp concrete.

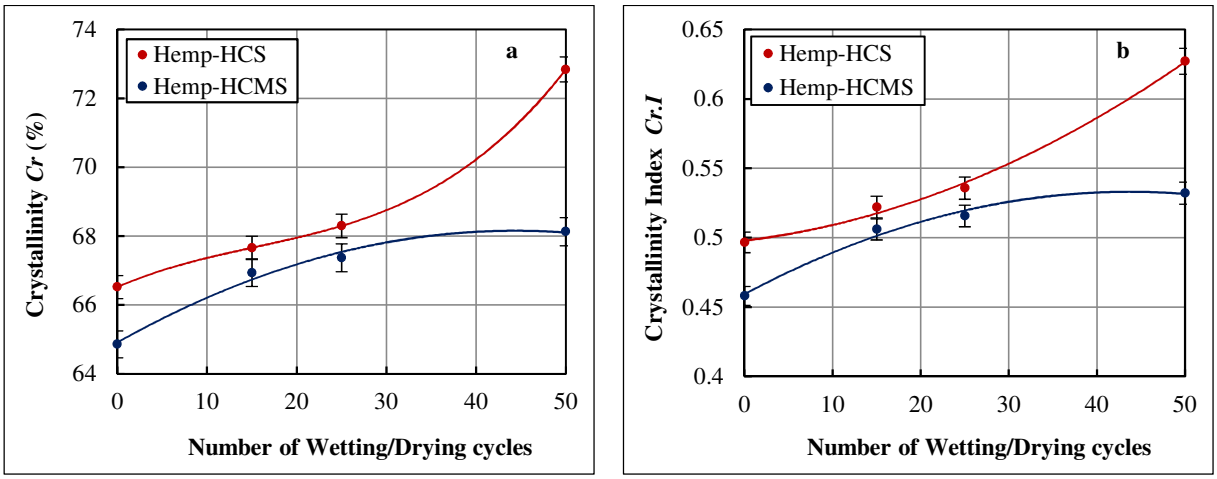

Fig. 20. Percentage of crystallinity (a) and Crystallinity Index (b) of pull-out hemp particles vs. aging cycles

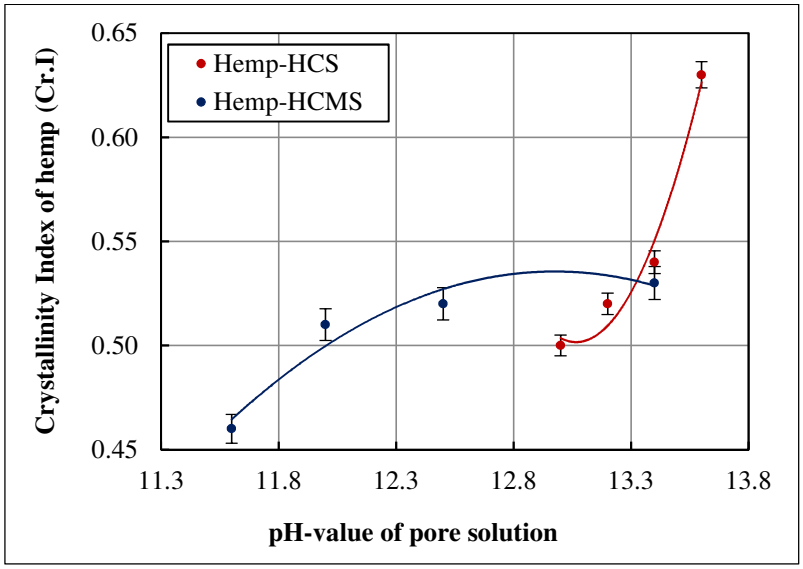

Fig. 21. Correlations between crystallinity index and pH value of pore solutions along aging cycles

The effectiveness of metakaolin in improving durability of hemp concrete has been assessed by examining the relationship between hemp particle degradation degree and the loss of mechanical properties of hemp concrete. Fig. 22 shows the correlations between crystallinity index and compressive/flexural post-cracking toughness of hemp concrete. A noticeable influence of crystallinity properties of embedded hemp on degradation degree of hemp concrete is evidenced. However, as the *Cr. I* of embedded hemp increased, the loss of toughness increases. These results indicated that the use of metakaolin as partial replacement of lime binder is an effective means to improve durability of hemp concrete through the restraint of hemp particle degradation. It's concluded that in order to prevent the degradation of vegetable materials in alkaline medium, amorphous components (lignin, hemicellulose, and cellulose) should be protected by reducing alkalinity of pore solution in the matrix through the modification of hydration products.

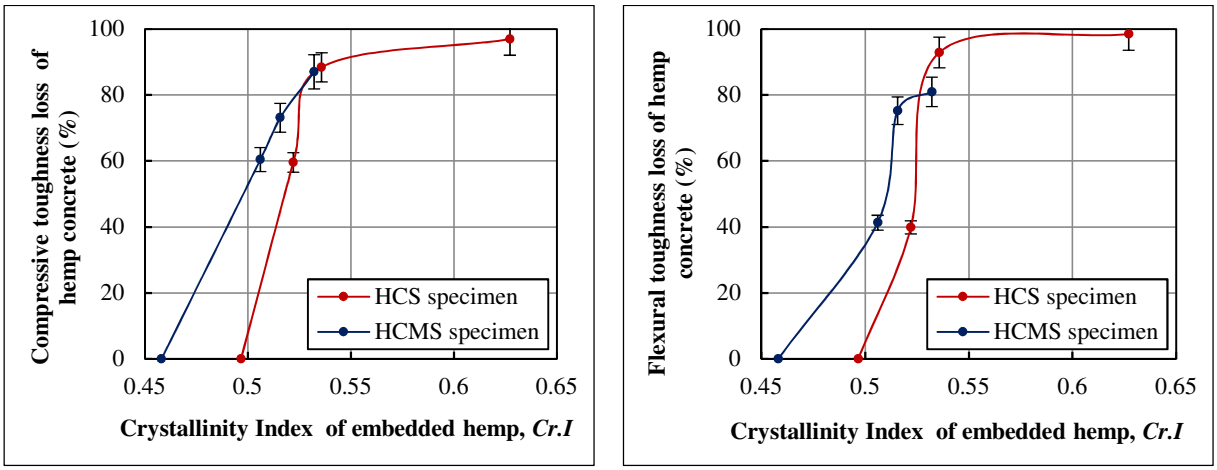

Fig. 22. Correlations between crystalline properties of hemp particles and mechanical behavior of hemp concrete

4 Conclusion

This study reports the investigation of effective means leading to improve durability of hemp concrete based commercial lime binder when subjected to accelerated aging conditions of wetting and drying cycle, through a partial substitution of binder-based lime by metakaolin. The degradation degree of specimen was investigated by testing the residual physico-mechanical properties after 0, 15, 25, and 50 of wetting/drying cycling exposures.

The results have shown the effectiveness of metakaolin addition to minimise the degradation of hemp concrete, particularly after 25th cycle. The pozzolanic reaction should contribute towards durability of the specimen, which results in improvement of both matrix strength and hemp-binder bond as evidenced by SEM micrographs analysis. Furthermore, a reduction in the porosity of the binder due to the increase in amount of pozzolanic products also leads to minimise vulnerability of specimens. The micro-analyses have also shown that the pozzolanic reaction appears to significantly restrain hemp particle degradation, due to the reduction in the alkaline degree of the binder medium. The relationship between hemp particle degradation and the loss of the mechanical properties of hemp concrete indicates that the use of metakaolin is an effective means to improve durability of hemp concrete through the restraint of hemp particle degradation. It is concluded that the combination of metakaolin and commercial lime binder appears to enhance interfacial bond strength of hemp particles to the matrix, due to both additional production of C-S-H gel and protective effect of hemp particles as regards the mineralisation mechanism and alkali attack. However, the effect of alkalinity of pore solution on the vegetable particle degradation could be used as important factors to predict the damage of hemp concrete subjected to aging conditions.

The effectiveness of pozzolane addition on the properties of hemp concrete as regards its hygro-thermal performances, after wetting/drying cycling exposure, need to be investigated. A part of this study is in progress.

References

1. *EU energy, transport and GHG emissions trends to 2050 reference scenario*, ed. E. Europäische Kommission Generaldirektion. 2014: Publ. Off. of the Europ. Union.
2. Saghrouni, Z., D. Baillis, and A. Jemni, *Composites based on Juncus maritimus fibers for building insulation.* Cement and Concrete Composites, 2020. **106**: p. 103474.
3. Ajouguim, S., et al., *Effect of Alfa fibers on the mechanical and thermal properties of compacted earth bricks.* Materials Today: Proceedings, 2021. **37**: p. 4049-4057.
4. Benmahiddine, F., et al., *Effect of flax shives content and size on the hygrothermal and mechanical properties of flax concrete.* Construction and Building Materials, 2020. **262**: p. 120077.
5. SaravanaKumar, M., et al., *Influence of fiber loading on mechanical characterization of pineapple leaf and kenaf fibers reinforced polyester composites.* Materials Today: Proceedings, 2021. **46**: p. 439-444.
6. Islam, M.S. and S.J.U. Ahmed, *Influence of jute fiber on concrete properties.* Construction and Building Materials, 2018. **189**: p. 768-776.
7. Stanwix, W. and A. Sparrow, *The Hempcrete Book: Designing and Building with Hemp-lime*. 2014: Green Books.
8. Benmahiddine, F. and R. Belarbi. *Effect of Immersion/Freezing/Drying Cycles on the Hygrothermal and Mechanical Behaviour of Hemp Concrete*. in *Construction Technologies and Architecture*. 2022. Trans Tech Publ.
9. Arnaud, L. and E. Gourlay, *Experimental study of parameters influencing mechanical properties of hemp concretes.* Construction and Building Materials, 2012. **28**(1): p. 50-56.
10. Williams, J., M. Lawrence, and P. Walker, *A method for the assessment of the internal structure of bio-aggregate concretes.* Construction and Building Materials, 2016. **116**: p. 45-51.
11. Ingrao, C., et al., *Energy and environmental assessment of industrial hemp for building applications: A review.* Renewable and Sustainable Energy Reviews, 2015. **51**: p. 29-42.
12. Walker, R., et al., *Mechanical properties and durability of hemp-lime concretes.* 2014. **61**: p. 340-348.
13. Le, A.T., et al., *Influence of various starch/hemp mixtures on mechanical and acoustical behavior of starch-hemp composite materials.* Composites Part B: Engineering, 2015. **75**: p. 201-211.
14. Arizzi, A., et al., *Optimization of lime and clay-based hemp-concrete wall formulations for a successful lime rendering.* 2018. **184**: p. 76-86.
15. Nguyen, S., et al., *Modeling thermal conductivity of hemp insulation material: A multi-scale homogenization approach.* 2016. **107**: p. 127-134.
16. Binici, H., et al., *Mechanical, thermal and acoustical characterizations of an insulation composite made of bio-based materials.* 2016. **20**: p. 17-26.
17. Mazhoud, B., et al., *Effect of hemp content and clay stabilization on hygric and thermal properties of hemp-clay composites.* Construction and Building Materials, 2021. **300**: p. 123878.
18. Latif, E., et al., *Moisture buffer potential of experimental wall assemblies incorporating formulated hemp-lime.* 2015. **93**: p. 199-209.
19. Lelievre, D., et al., *Hygrothermal behavior of bio-based building materials including hysteresis effects: Experimental and numerical analyses.* 2014. **84**: p. 617-627.
20. Benmahiddine, F., et al., *Experimental investigation on the influence of immersion/drying cycles on the hygrothermal and mechanical properties of hemp concrete.* Journal of Building Engineering, 2020. **32**: p. 101758.
21. Araya-Letelier, G., et al., *Experimental evaluation of adobe mixtures reinforced with jute fibers.* Construction and Building Materials, 2021. **276**: p. 122127.
22. Saloni, et al., *Influence of Portland cement on performance of fine rice husk ash geopolymer concrete: Strength and permeability properties.* Construction and Building Materials, 2021. **300**: p. 124321.
23. Zaid, I., M. Merzoud, and A. Benazzouk, *Morphological and mineralogical analysis of treated Diss fibers and their effect on physico-mechanical characteristics of Diss concrete based on alternative binder.* Construction and Building Materials, 2021. **307**: p. 124936.
24. Dušek, J., et al., *Sustainable composite material based on surface-modified rape straw and environment-friendly adhesive.* Construction and Building Materials, 2021. **300**: p. 124036.
25. Gram, H.E. *Durability of natural fibres in concrete*. 1984.
26. Bilba, K. and M.A. Arsene, *Silane treatment of bagasse fiber for reinforcement of cementitious composites.* Composites Part A: Applied Science and Manufacturing, 2008. **39**(9): p. 1488-1495.
27. Tolêdo Filho, R.D., et al., *Development of vegetable fibre–mortar composites of improved durability.* Cement and Concrete Composites, 2003. **25**(2): p. 185-196.
28. Mohr, B.J., H. Nanko, and K.E. Kurtis, *Durability of kraft pulp fiber–cement composites to wet/dry cycling.* Cement and Concrete Composites, 2005. **27**(4): p. 435-448.
29. Pavasars, I., et al., *Alkaline Degradation of Cellulose: Mechanisms and Kinetics.* Journal of Polymers and the Environment, 2003. **11**(2): p. 39-47.

30. Tonoli, G.H.D., et al., *Effects of natural weathering on microstructure and mineral composition of cementitious roofing tiles reinforced with fique fibre.* Cement and Concrete Composites, 2011. **33**(2): p. 225-232.
31. Bentchikou, M., et al., *Effect of recycled cellulose fibres on the properties of lightweight cement composite matrix.* Construction and Building Materials, 2012. **34**: p. 451-456.
32. Ardanuy, M., et al., *Fiber-matrix interactions in cement mortar composites reinforced with cellulosic fibers.* Cellulose, 2011. **18**(2): p. 281-289.
33. Claramunt, J., et al., *The hornification of vegetable fibers to improve the durability of cement mortar composites.* Cement and Concrete Composites, 2011. **33**(5): p. 586-595.
34. Morton, J.H., T. Cooke, and S.A.S. Akers, *Performance of slash pine fibers in fiber cement products.* Construction and Building Materials, 2010. **24**(2): p. 165-170.
35. Toledo Filho, R.D., et al., *Free, restrained and drying shrinkage of cement mortar composites reinforced with vegetable fibres.* Cement and Concrete Composites, 2005. **27**(5): p. 537-546.
36. Hakamy, A., F.U.A. Shaikh, and I.M. Low, *Effect of calcined nanoclay on the durability of NaOH treated hemp fabric-reinforced cement nanocomposites.* Materials & Design, 2016. **92**: p. 659-666.
37. Pehanich, J.L., P.R. Blankenhorn, and M.R. Silsbee, *Wood fiber surface treatment level effects on selected mechanical properties of wood fiber–cement composites.* Cement and Concrete Research, 2004. **34**(1): p. 59-65.
38. Mohr, B.J., J.J. Biernacki, and K.E. Kurtis, *Supplementary cementitious materials for mitigating degradation of kraft pulp fiber-cement composites.* Cement and Concrete Research, 2007. **37**(11): p. 1531-1543.
39. Soroushian, P., J.-P. Won, and M. Hassan, *Durability characteristics of CO2-cured cellulose fiber reinforced cement composites.* Construction and Building Materials, 2012. **34**: p. 44-53.
40. Mohr, B.J., H. Nanko, and K.E. Kurtis, *Durability of thermomechanical pulp fiber-cement composites to wet/dry cycling*. Cement and Concrete Research, 2005. **35**(8): p. 1646-1649.
41. Khorami, M. and E. Ganjian, *The effect of limestone powder, silica fume and fibre content on flexural behaviour of cement composite reinforced by waste Kraft pulp.* Construction and Building Materials, 2013. **46**: p. 142-149.
42. Mohr, B.J., J.J. Biernacki, and K.E. Kurtis, *Microstructural and chemical effects of wet/dry cycling on pulp fiber–cement composites.* Cement and Concrete Research, 2006. **36**(7): p. 1240-1251.
43. BCB-Tradical, *Chaux formulée pour Maçonner et Dégrossir et Bétons de Chanvre Tradical*. 2016.
44. CERADEL, *ARGICALTM – M 1000. Metakaolin*. 2014.
45. Schneider, C.A., W.S. Rasband, and K.W.J.N.m. Eliceiri, *NIH Image to ImageJ: 25 years of image analysis.* 2012. **9**(7): p. 671-675.
46. Bourdot, A., et al., *Characterization of a hemp-based agro-material: Influence of starch ratio and hemp shive size on physical, mechanical, and hygrothermal properties.* 2017. **153**: p. 501-512.
47. Rahim, M., et al., *Characterization of flax lime and hemp lime concretes: Hygric properties and moisture buffer capacity.* Energy and Buildings, 2015. **88**: p. 91-99.
48. Tradical-BCB, *Tradical THERMO Formulated limes for Tradical Hempcretes*. 2017.
49. Designation, A., *C20-00 Standard Test Methods for Apparent Porosity.* Water Absorption, Apparent Specific Gravity and Bulk Density of Burned Refractory Brick and Shapes by Boiling Water.
50. van der Sloot, H.A., *Comparison of the characteristic leaching behavior of cements using standard (EN 196-1) cement mortar and an assessment of their long-term environmental behavior in construction products during service life and recycling.* Cement and Concrete Research, 2000. **30**(7): p. 1079-1096.
51. Wei, J. and C. Meyer, *Degradation mechanisms of natural fiber in the matrix of cement composites.* Cement and Concrete Research, 2015. **73**: p. 1-16.
52. Wei, J. and C.J.C.S. Meyer, *Degradation of natural fiber in ternary blended cement composites containing metakaolin and montmorillonite.* 2017. **120**: p. 42-60.
53. Alonso, M.C., et al., *Development and application of low-pH concretes for structural purposes in geological repository systems*, in *Geological Repository Systems for Safe Disposal of Spent Nuclear Fuels and Radioactive Waste*, J. Ahn and M.J. Apted, Editors. 2010, Woodhead Publishing. p. 286-322.
54. Roy, A., et al., *Improvement in mechanical properties of jute fibres through mild alkali treatment as demonstrated by utilisation of the Weibull distribution model.* Bioresource Technology, 2012. **107**: p. 222-228.
55. Gill, A.S. and R. Siddique, *Durability properties of self-compacting concrete incorporating metakaolin and rice husk ash.* Construction and Building Materials, 2018. **176**: p. 323-332.
56. Sabir, B.B., S. Wild, and J. Bai, *Metakaolin and calcined clays as pozzolans for concrete: a review.* Cement and Concrete Composites, 2001. **23**(6): p. 441-454.
57. Akhavan, A., J. Catchmark, and F. Rajabipour, *Ductility enhancement of autoclaved cellulose fiber reinforced cement boards manufactured using a laboratory method simulating the Hatschek process.* Construction and Building Materials, 2017. **135**: p. 251-259.

58. Ballesteros, J.E.M., et al., *Synergic effect of fiber and matrix treatments for vegetable fiber reinforced cement of improved performance.* Construction and Building Materials, 2019. **205**: p. 52-60.
59. Pacheco-Torgal, F. and S. Jalali, *Cementitious building materials reinforced with vegetable fibres: A review.* Construction and Building Materials, 2011. **25**(2): p. 575-581.
60. Silva, F.d.A., et al., *Effect of fiber shape and morphology on interfacial bond and cracking behaviors of sisal fiber cement based composites.* 2011. **33**: p. 814-823.
61. El Achaby, M., et al., *Processing and properties of eco-friendly bio-nanocomposite films filled with cellulose nanocrystals from sugarcane bagasse.* 2017. **96**: p. 340-352.
62. Tolêdo Filho, R.D., et al., *Durability of alkali-sensitive sisal and coconut fibres in cement mortar composites.* Cement and Concrete Composites, 2000. **22**(2): p. 127-143.
63. Agopyan, V., et al., *Developments on vegetable fibre-cement based materials in Sao Paulo, Brazil: an overview.* 2005. **27**: p. 527-536.
64. Tonoli, G.H.D., et al., *Surface properties of eucalyptus pulp fibres as reinforcement of cement-based composites.* Holzforschung, 2010. **64**: p. 595-601.
65. Toledo Filho, R.D., et al., *Durability of compression molded sisal fiber reinforced mortar laminates.* Construction and Building Materials, 2009. **23**(6): p. 2409-2420.
66. Le Troedec, M., et al., *Influence of various chemical treatments on the composition and structure of hemp fibres.* Composites Part A: Applied Science and Manufacturing, 2008. **39**(3): p. 514-522.